Published in final edited form as:

Neuron. 2017 September 13; 95(6): 1365–1380.e5. doi:10.1016/j.neuron.2017.08.022.

Connexin 43-mediated astroglial metabolic networks contribute to the regulation of the sleep-wake cycle

Jerome Clasadonte[1,2,3,*], **Eliana Scemes**[4], **Zhongya Wang**[5], **Detlev Boison**[5], and **Philip G. Haydon**[1,6,*]

[1]Department of Neuroscience, Tufts University School of Medicine, Boston, MA 02111, USA

[2]Inserm, Laboratory of Development and Plasticity of the Neuroendocrine Brain, Jean-Pierre Aubert Research Center, U1172, Lille, France

[3]University of Lille, FHU 1000 days for Health, School of Medicine, Lille, France

[4]Dominick P. Purpura Department of Neuroscience, Albert Einstein College of Medicine, Bronx, NY 10461, USA

[5]Robert Stone Dow Neurobiology Laboratories, Legacy Research Institute, Portland, OR 97232 USA

Summary

Astrocytes produce and supply metabolic substrates to neurons through gap junction-mediated astroglial networks. However, the role of astroglial metabolic networks in behavior is unclear. Here, we demonstrate that perturbation of astroglial networks impairs the sleep-wake cycle. Using a conditional Cre-Lox system in mice, we show that knockout of the gap junction subunit connexin 43 in astrocytes throughout the brain causes excessive sleepiness and fragmented wakefulness during the nocturnal active phase. This astrocyte-specific genetic manipulation silenced the wake-promoting orexin neurons located in the lateral hypothalamic area (LHA) by impairing glucose and lactate trafficking through astrocytic networks. This global wakefulness instability was mimicked with viral delivery of Cre recombinase to astrocytes in the LHA and rescued by *in vivo* injections of lactate. Our findings propose a novel regulatory mechanism critical for maintaining normal daily cycle of wakefulness and involving astrocyte-neuron metabolic interactions.

Keywords

Astrocytic metabolic networks; gap junction; lactate; orexin neuron; sleep-wake cycle; EEG

[*]Correspondence: philip.haydon@tufts.edu (P.G.H.), jerome.clasadonte@inserm.fr (J.C.).
[6]Lead Contact.

Author Contributions

J.C. and P.G.H. designed and supervised research. J.C. and E.S. performed research. J.C. analyzed data. Z.W. and D.B. contributed new reagents. J.C. and P.G.H. wrote the paper.

Introduction

Sleep plays a vital role in health and well-being, and is critical for immune function, metabolism, and memory and learning (Brown et al., 2012). While major progress has been made in understanding functions of sleep, mechanisms underlying its regulation are unclear (Brown et al., 2012). It was only recently that astrocytes have been implicated in sleep mechanisms and functions through their regulation of gliotransmission (Halassa et al., 2009; Paukert et al., 2014; Araque et al., 2014).

Astrocytes form an extensive network of cells interconnected through gap junction channels formed by connexin (Cx) proteins (Goodenough et al., 1996). Gap junctions allow the passage of small molecules including, ions, second messengers and energy metabolites such as glucose and lactate (see Giaume et al., 2010). Cx43, the major constituent of gap junctions in astrocytes, is highly expressed throughout the brain (Nagy and Rash, 2000). The Cre-Lox conditional knockout (cKO) approach is often used to investigate the physiological functions of astroglial Cx43 and astrocytic networks in the CNS (Giaume et al., 2010; Giaume and Theis, 2010; Pannasch and Rouach, 2013; Oliveira et al., 2015). The use of Cx43 cKO^{GFAP} mice with Cre transgenic lines under the promoter of a human glial fibrillary acidic protein ($Cx43^{f/f}$:hGFAP-Cre; Theis et al., 2003; Wiencken-Barger et al., 2007) has demonstrated the contribution of Cx43 hemichannels and Cx43-mediated gap junctions to neuron-glia interactions (Giaume et al., 2010; Giaume and Theis, 2010; Pannasch and Rouach, 2013, Oliveira et al., 2015), and to metabolic coupling between neurons and astrocytes (Rouach et al., 2008). This latter process is based on the “astrocyte to neuron lactate shuttle” (ANLS) hypothesis (Pellerin and Magistretti, 1994), in which glucose is taken up by astrocyte endfeet, enters the glycolytic pathway to be converted into lactate, which is then transported through the gap junction-mediated astrocytic network to fuel neuronal energy demands (Rouach et al., 2008). Although recent studies suggest a role for astroglial Cx43 in neuroglial interactions, their contribution to physiological brain functions such as sleep remains largely unknown.

We performed cortical electroencephalographic (EEG) and electromyographic (EMG) recordings in Cx43 cKO^{GFAP} mice (Wiencken-Barger et al., 2007; Han et al., 2014) to determine the role of astroglial Cx43 on sleep-wake regulation. Cx43 cKO^{GFAP} mice exhibited excessive sleepiness and fragmented wakefulness during the nocturnal active phase. We show that orexin (hypocretin)-producing neurons (orexin neurons) in the lateral hypothalamic area (LHA), crucial regulators of wakefulness (Sakurai, 2007), have reduced excitability in Cx43 cKO^{GFAP} mice. This reduced activity was due to an attenuated diffusion of energy metabolites, glucose and lactate, through gap junction-mediated astrocytic networks in the LHA. Viral transduction of astrocytes in the LHA of $Cx43^{f/f}$ littermate controls mimicked the sleep phenotype of cKO animals by promoting sleepiness and fragmented wakefulness during the nocturnal active phase. This phenotype was rescued by chronic delivery of lactate into the LHA. We demonstrate that an astrocytic source of lactate trafficking through the Cx43-mediated astrocytic gap junctions in the LHA is crucial for normal activity of orexin neurons and, consequently, for wakefulness.

Results

Deletion of Cx43 in astrocytes decreases wakefulness during the active phase

To investigate the role of astroglial Cx43 in sleep-wake regulation, we combined cortical EEG and EMG recordings with the $Cx43^{f/f}$:hGFAP-Cre mouse (Wiencken-Barger et al., 2007; Han et al., 2014), which allowed us to knockout the *Gja1* gene encoding Cx43 selectively in astrocytes. To generate $Cx43^{f/f}$:hGFAP-Cre (Cx43 cKO^{GFAP}) mice, homozygous $Cx43^{f/f}$ mice (Liao et al., 2001) were crossed to hGFAP-Cre mice (Casper and McCarthy, 2006), in which the Cre recombinase is under the control of the human glial GFAP promoter (Figure 1A). PCR was used to identify the correct genotypes (Figure 1B) and the efficiency and specificity of *Gja1* gene deletion in astrocytes in the Cx43 cKO^{GFAP} mice were characterized previously (Wiencken-Barger et al., 2007; Han et al., 2014). Western blots demonstrated that Cx43 expression was substantially reduced in brains of Cx43 cKO^{GFAP} mice compared to $Cx43^{f/f}$ littermates and WT mice with the same C57BL/6J inbred background (Figure 1C).

EEG/EMG recordings for 24h indicated that $Cx43^{f/f}$ and Cx43 cKO^{GFAP} mice displayed a normal circadian sleep-wake rhythm (Figure 1D). However, Cx43 cKO^{GFAP} mice showed changes in vigilance state distribution during the dark phase (Figure 1D). The time spent awake in Cx43 cKO^{GFAP} mice was reduced by 23.76% during the 12h dark phase, when mice are typically active (Figure 1E). This reduction was concomitant with a significant increase in time spent in non-rapid eye movement (NREM) sleep (56.73%), rapid eye movement (REM) sleep (141.88%) and total sleep time (TST including REM+NREM sleep: 59.79%; Figure 1E). These results indicate that deficiency in astroglial Cx43 induces sleepiness during the nocturnal active phase.

Cx43 deletion in astrocytes causes wakefulness instability during the active phase

Cx43 cKO^{GFAP} were unable to sustain a period of consolidated wakefulness especially during the first 6h of the dark phase (zeitgeber time (ZT) 12-ZT18; Figure 1F). Intrusions of short periods of NREM sleep were frequently found within periods of wakefulness at the beginning of the dark phase (Figure 1F). In addition, Cx43 cKO^{GFAP} mice had more episodes of wakefulness during both light and dark phases (Figure 1G), although of shorter duration (Figure 1H). Cx43 cKO^{GFAP} mice also had more episodes of NREM and REM sleep but only during the dark phase (Figure 1G) and with a duration that remained unchanged (Figure 1H). This increase in episode numbers of wakefulness, NREM and REM sleep in Cx43 cKO^{GFAP} mice during dark phase was associated with an increase in the number of transitions between all vigilance states (Figure 1I), demonstrating that these mice had difficulty in sustaining long episodes of wakefulness.

Cx43 deletion in astrocytes decreases spontaneous firing frequency and excitability in orexin neurons

Since excessive sleepiness and instability of wakefulness during the active phase is reminiscent of narcolepsy due to the loss of wake-promoting orexin neurons in the LHA (Sakurai, 2007), we investigated whether Cx43 cKO^{GFAP} mice caused changes in orexin neurons. Immunohistochemistry, against orexin (ORX)-A, the main isoform of orexin

involved in the regulation of wakefulness (Sakurai, 2007), showed that the number of ORX-A positive cells was similar in both genotypes (Figure S1).

Since electrical activity of orexin neurons changes across the sleep-wake cycle (Mileykovskiy et al., 2005; Lee et al., 2005; Adamantadis et al., 2007; Hassani et al., 2009; Tsunematsu et al., 2011), we used whole-cell current-clamp recordings in acute brain slices to ask whether astroglial Cx43 modulates the activity of orexin neurons. Orexin neurons were identified based on their electrophysiological characteristics (Eggermann et al., 2003; Parsons and Hirasawa, 2010) such as tonic spontaneous firing (Figure 2A1), H-current (Figure S2A), monophasic after hyperpolarizing potential (AHP; Figure S2A) and low-threshold spike (Figure S2A). Recorded cells were filled with biocytin for *post hoc* histological verification of ORX-A-expressing neurons (Figures 2A2 and 2B2). With an artificial cerebrospinal fluid (ACSF) containing physiological concentration of glucose (2.5mM; Parsons and Hirasawa, 2010; Sada et al., 2015), orexin neurons from Cx43 cKO^{GFAP} mice displayed reduced spontaneous firing compared with $Cx43^{f/f}$ mice (Figures 2A1, 2B1 and 2C). This reduced basal firing persisted in loose patch-clamp configuration (Figures 2D–2F), indicating that it was not a consequence of dilution of the intracellular compartment by whole-cell dialysis.

In Cx43 cKO^{GFAP} mice, orexin neurons fired fewer action potentials in response to depolarizing injected currents compared to $Cx43^{f/f}$ mice (Figures 2G, 2H, S2A and S2B). The rate of increase in firing frequency during current ramps from 0 to +50pA was decreased by 36% in orexin neurons from Cx43 cKO^{GFAP} mice ($Cx43^{f/f}$, 0.30±0.01 Hz/pA; n=15 cells, 9 mice; Cx43 cKO^{GFAP}, 0.19±0.01 Hz/pA; n=11 cells, 7 mice; Student t-test, $p<0.001$; Figures 2G and 2H) while the slope of the action potential (AP) output in response to current injection was decreased by 23% ($Cx43^{f/f}$, 0.34±0.02 AP/pA; n=14 cells, 9 mice; Cx43 cKO^{GFAP}, 0.26±0.02 AP/pA; n=12 cells, 6 mice; Student t-test, $p<0.05$; Figure S2B). A more hyperpolarized resting membrane potential (RMP; Figure S2C) as well as a lower membrane input resistance (R_{in}; Figure S2D) were also observed in orexin neurons from the cKO animals. The slope of the current-voltage relationship from cKO animals was decreased compared with littermate controls (Figures S2A and S2E), resulting in the convergence of the two curves at −88 mV (Figure S2E), which is close to the potassium equilibrium potential in our conditions, suggesting that this effect was mediated by a potassium conductance.

Orexin neurons use lactate as energy substrate

It has been previously suggested that orexin neurons rely on lactate as their main energy source (Parsons and Hirasawa, 2010). Since Cx43 gap junctions are critical for the trafficking of glucose and its metabolite, lactate, through the astrocytic networks during neuronal activity (Rouach et al., 2008), we hypothesized that the reduced activity of orexin neurons observed in Cx43 cKO^{GFAP} mice could result from a deficiency in the diffusion of energy substrates between astrocytes in the LHA.

To confirm that orexin neurons in $Cx43^{f/f}$ littermate controls use lactate as energy substrate, we used the selective blocker of monocarboxylate transporters (MCTs), α-cyano-4-hydroxycinnamate (4-CIN) to block the lactate influx into neuronal cells (Parsons and

Hirasawa, 2010). In the presence of physiological levels of glucose (2.5 mM), bath application of 4-CIN (500μM) induced a reversible membrane hyperpolarization of 9.71±1.47 mV (n=7 cells, 3 mice) that was sufficient to inhibit the tonic firing of orexin neurons (Figures 3A and 3B). To test whether exogenous lactate was sufficient to sustain the activity of orexin neurons, we induced glucose deprivation by switching from 2.5 to 0mM glucose in ACSF. This caused a membrane hyperpolarization (from −55.25±1.69 mV to −66.37±1.98 mV; n=8 cells, 6 mice; Paired Student t-test, $p<0.001$) that was sufficient to inhibit the activity of orexin neurons (Figures 3C and 3D). During glucose deprivation, bath application of 5mM lactate (equicaloric to 2.5mM glucose; Parsons and Hirasawa, 2010), restored both the basal membrane potential (−54.50±2.37 mV; n=6 cells, 3 mice; Student t-test, $p>0.05$) and spontaneous firing frequency of orexin neurons (Figures 3C and 3D). The recovering effect of lactate on orexin neuron activity during glucose deprivation was abrogated when slices were perfused with 500μM 4-CIN (Figures 3C and 3D), suggesting that the excitatory effect of lactate required its transport through the cell membrane. The requirement for lactate being transported into the neuron, rather than acting on an extracellular receptor (Tang et al., 2014), was confirmed by performing additional recordings with a patch pipette solution containing lactate under conditions of energy depletion. Dialysis of orexin neurons with 2.5mM lactate in whole-cell configuration for 20–30min after break-in prevented the inhibitory effects of either glucose deprivation or 4-CIN (Figures 3E and 3F). Together, these data suggest that orexin neuronal activity is primarily dependent on lactate uptake.

Based on the ANLS hypothesis, lactate produced from astrocytic glucose and taken up by neurons via MCTs, mediates its effect through lactate dehydrogenase (LDH), an enzyme responsible for conversion of lactate to pyruvate, the downstream metabolite that enters the tricarboxylic cycle to fuel neurons (Pellerin and Magistretti, 1994; Bellanger et al., 2011; Lam et al., 2005; Sada et al., 2015). In favor of this hypothesis, we found that bath application of pyruvate (5mM), which can also be transported into the cells by MCTs (Halestrap and Price, 1999), rescued the inhibitory effect of glucose deprivation on orexin neurons, an action that was suppressed by 500μM 4-CIN (Figures 3G and 3H). Also, inhibition of LDH by bath application of 10mM oxamate (Sada et al., 2015), to prevent the conversion of lactate to pyruvate, hyperpolarized orexin neurons (from −54.42±1.75 mV to −67.14±1.38 mV; n=7 cells, 3 mice; Paired Student t-test, $p<0.001$) and strongly suppressed their spike firing (Figures 3I–3K), mimicking the inhibitory effect of glucose deprivation (Figures 3C, 3D, 3G and 3H). Finally, membrane hyperpolarization and loss of activity induced by oxamate were both fully restored by bath application of pyruvate (5mM), the downstream metabolite of LDH (membrane potential in the presence of oxamate+pyruvate, −52.00±1.43 mV; n=8 cells, 3 mice; Student t-test, $p>0.05$; Figures 3J and 3K), but not by the addition of lactate (5mM), the upstream substrate of LDH (membrane potential in presence of oxamate+lactate, −66.16±2.32 mV; n=6 cells, 3 mice; Student t-test, $p<0.01$; Figures 3I and 3K). These results indicate that lactate mediates its excitatory effects on orexin neurons through the activity of the LDH enzyme, a metabolic component of the ANLS.

What is the mechanism for the effect of lactate on membrane potential and spontaneous tonic firing of orexin neurons? We found that the membrane hyperpolarization induced by

glucose deprivation (from −47.33±3.38 mV to −61.67±5.36 mV; n=3 cells, 3 mice; Paired Student t-test, $p<0.05$) persisted under 0.5μM tetrodotoxin (Figure S3A), suggesting a direct postsynaptic effect. The membrane hyperpolarization was caused by activation of a current that reversed near the potassium equilibrium potential (−83.38±8.18 mV, n=4 cells, 3 mice; Figures S3B1 and S3B2). We next observed that the inhibitory effect of glucose deprivation was either restored (Figures S3C and S3D) or prevented (Figures S3E and S3G) by bath application of tolbutamide (100μM), a blocker of ATP-sensitive potassium (K_{ATP}) channels (Sada et al., 2015), suggesting that K_{ATP} channels mediated the inhibition of orexin neurons. To confirm that maintenance of orexin neuron activity by lactate, and to some extent by pyruvate, involves K_{ATP} channels, we tested the effect of tolbutamide on 4-CIN- and oxamate-induced inhibition of orexin neurons. Pre-treatment of slices with tolbutamide (100μM) for at least 15min completely abolished the inhibitory effect caused by 500μM 4-CIN and 10mM oxamate (Figures S3E–S3G). Consistent with previous studies (Parsons and Hirasawa, 2010), these results indicate that lactate sustains tonic spontaneous activity of orexin neurons by modulating K_{ATP} channel activity.

We asked whether the delivery of lactate into a single astrocyte in the LHA could rescue normal activity of orexin neurons during glucose deprivation. A single astrocyte was dialyzed with 5mM lactate while performing whole-cell recording from a distant orexin neuron (50–75μm apart; Figures 4A and 4B). When astrocytes were dialyzed with lactate, glucose-deprivation no longer induced a reduction in action potential firing nor a membrane hyperpolarization (Figures 4C–4F). This preventive effect of lactate was suppressed by 4-CIN (500μM; Figures 4D–4F), indicating that transcellular transport of lactate through MCTs was required for its effect. These data show that shuttling of lactate from astrocytes to neurons is functional in the LHA and contributes to the tonic firing of orexin neurons.

Gap junction-mediated astrocytic networks are functional in the LHA

Gap junction-mediated astrocytic networks are functional in the LHA since injection of biocytin (Rouach et al., 2008), into a single astrocyte diffused from the patch pipette extensively into neighboring astrocytes (Figures 5A and 5D). This intercellular diffusion was significantly attenuated by the gap junction blocker, carbenoxolone (CBX; 50μM; Rouach et al., 2008, Figures 5C and 5D). Most coupled cells were immunopositive for the astrocyte marker GFAP, but not for the neuronal marker NeuN (Figure 5E), suggesting a lack of dye-coupling between astrocytes and neurons in the LHA. When orexin neurons were recorded, biocytin was always restricted to the recorded cell (Figures 2A2 and 2B2), showing a lack of intercellular communication between astrocytes and orexin neurons. Together, these results demonstrate functional gap junctional coupling between astrocytes surrounding orexin neurons in the LHA.

We next studied the possibility for energy metabolites to traffic between astrocytes in the LHA by injecting the fluorescent glucose derivative 2-[N-(7-nitrobenz-2-oxa-1,3-diazol-4-yl)amino]-2-deoxyglucose (2-NBDG; Rouach et al., 2008) into a single LHA astrocyte via a patch pipette and analyzing its intercellular diffusion. Twenty min after break-in, 2-NBDG diffused from the patch pipette into neighboring astrocytes (Figures 5F and 5H).

Cx43 deletion in astrocytes weakens the astrocytic metabolic networks in the LHA

We next investigated by whole-cell recordings whether gap junctional coupling and trafficking of energy metabolites between astrocytes were altered in the LHA of Cx43 cKO^{GFAP}. Passive membrane properties of LHA astrocytes were similar between Cx43 cKO^{GFAP} and $Cx43^{f/f}$ mice (Figure S4). However, the number of dye-coupled LHA astrocytes following biocytin injection was reduced by 54.63% in Cx43 cKO^{GFAP} (Figures 5A, 5B and 5D). Similarly, the intercellular diffusion of 2-NBDG between LHA astrocytes was decreased by 52.12% in the cKO animals (Figures 5F–5H), indicating that glucose trafficking through the astrocytic network in the LHA requires Cx43.

Exogenous lactate restores the activity of orexin neurons in Cx43 cKO^{GFAP} mice

Given that orexin neuron activity relies on lactate, we asked whether exogenous lactate could restore the activity of these cells in Cx43 cKO^{GFAP} mice. In Cx43 cKO^{GFAP}, bath application of 5mM lactate in the presence of 2.5 mM glucose induced a membrane depolarization of 8.50±1.11 mV (n=8 cells, 4 mice) that was sufficient to restore the spontaneous activity of orexin neurons (Figures 6B and 6C). The recovery of spike firing by lactate was preserved during loose patch recordings (Figures 6E and 6F). Under the same treatment, the reduced excitability of orexin neurons in Cx43 cKO^{GFAP} mice also recovered and reached the level of that of orexin neurons from $Cx43^{f/f}$ mice (Cx43 cKO^{GFAP} + lactate, 0.26±0.03 Hz/pA; n=7 cells, 3 mice; $Cx43^{f/f}$, 0.29±0.03 Hz/pA; n=9 cells, 4 mice; Student t-test, $p>0.05$; Figures 6G–6J). Moreover, in orexin neurons from $Cx43^{f/f}$ mice, exogenous delivery of lactate (5mM) in the presence of 2.5mM glucose had no effect on the membrane potential (without lactate, −47.57±1.52 mV; with lactate, −47.00±1.41 mV; n=7 cells, 3 mice for each condition; Paired Student t-test, $p>0.05$; Figure 6A), spike frequency firing (Figures 6A, 6C, 6D and 6F) and cell excitability (without lactate, 0.29±0.03 Hz/pA; n=9 cells, 4 mice; with lactate, 0.28±0.03 Hz/pA; n=9 cells, 5 mice; Student t-test, $p>0.05$; Figures 6G and 6H). These results suggest that the decreased activity of orexin neurons in Cx43 cKO^{GFAP} results from a deficiency in the trafficking of glucose-derived lactate through the astrocytic network. Furthermore, pharmacological inhibition of the gap junction network with 50μM CBX in brain slices from $Cx43^{f/f}$ mice phenocopied those from Cx43 cKO^{GFAP} mice with reduced activity of orexin neurons (Figures 5I and 5J), which was recovered by exogenous supply of 5mM lactate (Figures 5I and 5J).

In vivo knockout of Cx43 in LHA astrocytes causes excessive sleepiness and fragmented wakefulness during the active phase

To determine whether the sleep-wake phenotype observed in Cx43 cKO^{GFAP} mice was specific to LHA astrocytes, we performed cortical EEG/EMG recordings in $Cx43^{f/f}$ mice bilaterally injected in the LHA with an AAV vector of serotype 8 carrying the construct hGfa2-Cre:GFP in which Cre recombinase, fused to green fluorescent protein (GFP; Matsuda and Cepko, 2007), is under the control of an astrocyte selective human hGfa2 promoter (Brenner et al., 1994; Lee et al., 2008), which is a truncated version of the GFAP promoter (Figure 7A). Three weeks after transduction of $Cx43^{f/f}$ mice with AAV, we observed efficient and selective expression of Cre:GFP in LHA astrocytes (Figures 7B, S5A and S5B). Out of 967 total GFP-expressing cells in the targeted LHA of transduced mice,

700 cells were positive for GFAP (72.38%, n=4; Figures S5A and S5B) and none were positive for ORX-A or NeuN (Figures S5A and S5B). Cortical EEG/EMG electrodes were implanted in transduced animals 10 days after the injection. EEG/EMG recordings started 4 days later for up to 7 days. On day 21 post-injection, sleep-wake parameters were compared with those of two different control groups of mice (Figure 7A) – (i) $Cx43^{f/f}$ mice injected bilaterally in the LHA with ACSF vehicle (n=4) and (ii) WT mice bearing the same C57BL/6J inbred background injected bilaterally in the LHA with AAV-hGfa2-Cre:GFP (n=4). Since the baseline 24h sleep-wake distribution (Figures S5C and S5D), the number and duration of vigilance state episodes (Figures S5E and S5F) and their number of transitions (Figure S5G) were similar in both control groups, we pooled them together as one control group. Compared with control mice, $Cx43^{f/f}$ mice transduced with AAV showed a decrease in time spent awake during the dark phase concomitant with an increase in the time spent in NREM sleep and TST (Figures 7C and 7D). In AAV-transduced $Cx43^{f/f}$ mice, wake episodes were frequently interrupted by short episodes of NREM sleep during the beginning of the dark phase from ZT12 to ZT18 (Figures 7E). These animals exhibited more wake episodes of shorter duration than controls (Figures 7F and 7G). The number of NREM sleep episodes was also increased in AAV-transduced $Cx43^{f/f}$ mice during the dark phase (Figure 7F) but without a change in their duration (Figure 7G). This nocturnal fragmented wakefulness was associated with an increase in the number of transitions from wake to NREM as well as from NREM to wake (Figure 7H). Thus, these data demonstrate that selective knockout of Cx43 in LHA astrocytes caused excessive sleepiness and instability of wakefulness during the nocturnal active phase, phenocopying the Cx43 cKO^{GFAP} mice.

Lactate delivery counteracts nocturnal wakefulness instability induced in $Cx43^{f/f}$ mice by the injection of AAV-hGfa2-Cre:GFP in the LHA

We asked whether *in vivo* delivery of lactate to the LHA would rescue the wakefulness instability induced in $Cx43^{f/f}$ mice by the transduction with AAV-hGfa2-Cre:GFP. We used osmotic minipumps to bilaterally introduce ACSF vehicle and subsequently lactate (5mM) in the LHA of the same individual $Cx43^{f/f}$ mice after implantation of cortical EEG/EMG electrodes and AAV-transduction (Figure 8A). Twenty-one days after AAV-hGfa2-Cre:GFP injection, $Cx43^{f/f}$ mice showed a change in the sleep-wake distribution characterized by a significant decrease in the time spent awake during the first 6h of the dark phase from ZT12 to ZT18 (Figures 8B and 8C), which was concomitant with a significant increase in the time spent in NREM sleep (Figures 8B and 8C) and TST (Figure 8C). This was accompanied by fragmented wakefulness (Figure 8D) characterized by increased number of wake episodes (Figure 8E) that were shorter in duration (Figure 8F). Transition number from wake to NREM and from NREM to wake were also increased after AAV-transduction (Figure 8G). While chronic infusion of ACSF for one week did not affect sleep-wake parameters in these animals (Figures 8B–8G), subsequent treatment with lactate for the same duration fully reversed the effects of AAV-transduction by restoring the sleep-wake distribution (Figures 8B and 8C), the number and duration of wake and NREM sleep episodes (Figures 8D–8F) and the number of transitions between wake and NREM sleep (Figure 8G). Thus, these results demonstrate that chronic *in vivo* delivery of lactate ameliorates nocturnal wakefulness instability induced by the loss of astroglial Cx43 in the LHA by restoring sustained wakefulness.

Discussion

Our results reveal an important role for astroglial Cx43 in sleep-wake regulation. We demonstrate that conditional deletion of Cx43 in astrocytes causes changes in sleep/wake patterns with disturbances of sleep and wakefulness. We found that Cx43 cKO^{GFAP} mice have reduced wakefulness concomitant with increased NREM sleep during the dark phase, at a time when mice, as nocturnal animals, would normally spend more time awake. Wakefulness in these animals was fragmented, frequently interrupted by short periods of NREM sleep. Consequently, Cx43 cKO^{GFAP} mice had increased episodes number for wake and NREM sleep and more frequent transitions from wake to sleep states and vice versa. These results reveal that Cx43 cKO^{GFAP} mice were unable to maintain persistent wakefulness during the normal wake phase.

Excessive sleepiness and instability in wakefulness may be a consequence of altered control of arousal-related brain regions. It is known that the LHA, which contains orexin neurons, plays a critical role in arousal stability (Sakurai, 2007). Notably, orexin deficiency has been linked to the chronic sleep disorder, narcolepsy, in animals (Lin et al., 1999; Chemelli et al., 1999; Willie et al., 2003; Mochizuki et al., 2004; Tabuchi et al., 2014) and humans (Peyron et al., 2000; Thannickal et al., 2000). Consistent with this, we found a dramatic decrease in the firing rate of orexin neurons in Cx43 cKO^{GFAP} mice, which could result in a reduced release of orexin (Kiyashchenko et al., 2002). This correlation between reduced electrical activity of orexin neurons and decreased wakefulness is supported by in vivo studies showing that firing frequency of orexin neurons varies according to the vigilance state, increasing during wakefulness and diminishing during NREM sleep (Mileykovskiy et al., 2005; Lee et al., 2005; Adamantadis et al., 2007; Hassani et al., 2009; Tsunematsu et al., 2011).

In agreement with a previous study (Parsons and Hirasawa, 2010), we confirmed that spontaneous firing of orexin neurons primarily relies on the uptake of lactate through MCTs. Furthermore, we demonstrate that the effect of lactate was mediated through activation of LDH, which converts lactate to the metabolite, pyruvate. We also found that lactate and pyruvate regulated firing and membrane potential of orexin neurons through the modulation of K_{ATP} channels, which have been shown to be expressed and functional in orexin neurons (Parsons and Hirasawa, 2010). Since LDH and K_{ATP} channels are well known to contribute to the metabolic regulation of neuronal excitation (Sada et al., 2015), our results allow us to confirm that orexin neurons preferentially use lactate rather than glucose as their source of energy to sustain neuronal activity.

In our study, we found that selective knockout of astroglial Cx43, which constitutes one of the molecular bases of astrocytic metabolic networks (Rouach et al., 2008), reduced dye-coupling between astrocytes in the LHA and perturbed the intercellular trafficking of glucose. As a consequence, orexin neurons had a decreased R_{in}, were hyperpolarized and displayed a dramatic reduction in spontaneous firing rate, likely due to the opening of K_{ATP} channels caused by a lowering of intracellular ATP levels. Consistent with this idea, exogenous supply of the energy metabolite, lactate, depolarized the membrane and restored the activity of orexin neurons. This supports the ANLS hypothesis in which lactate provided

by astrocytes represent the major source of energy for neurons (Pellerin and Magistretti, 1994; Bellanger et al., 2011). While we identified a major role for MCTs in the metabolic effect of lactate on orexin neurons, this does not rule out the implication of Cx43 hemichannels in this effect, since they may also mediate basal release of lactate from astrocytes (Stehberg et al., 2012; Karagiannis et al., 2015).

We also found that bilateral injection of AAV-hGfa2-Cre:GFP in the LHA of $Cx43^{f/f}$ mice recapitulated the Cx43 cKO^{GFAP} phenotype of excessive sleepiness and fragmented wakefulness during the nocturnal active phase, suggesting that this phenotype was specific to the LHA. Consistent with our *in vitro* results, wakefulness stability was fully restored by delivery of lactate into the LHA, confirming that the sleep phenotype was caused by energy-deprived orexin neurons. Given the importance of astroglial Cx43 in various brain areas and functions such as memory, emotion, motor coordination and sensory processing (Pannasch and Rouach, 2013; Oliveira et al., 2015), it is plausible that a deletion of astroglial Cx43 in another arousal nuclei may lead to a similar phenotype. This could be especially relevant in the locus coeruleus (LC) where astrocytic lactate acts on noradrenergic neurons as a signaling molecule to stimulate noradrenaline release (Tang et al., 2014).

Orexin neurons are strongly activated during the dark phase (Mileykovskiy et al., 2005; Lee et al., 2005; Hassani et al., 2009) and need a burst of fuel to heighten and maintain their tonic activity long enough to consolidate wakefulness. We show that the shuttling of energy metabolites through gap junction-mediated astrocytic networks is a prime candidate to efficiently provide this energy. Since each astrocyte can contact over 100,000 synapses (Bushong et al., 2002) and enwrap 4 to 8 neuronal somata (Halassa et al., 2007), the demand on one astrocyte for energy metabolite supply might be overwhelming. Thus, by increasing the effective volume of the intracellular compartment (De Pina-Benabou et al., 2001) and allowing glucose/lactate trafficking towards areas of high neuronal activity (Ball et al., 2007; Cruz et al., 2007; Rouach et al., 2008; Gandhi et al., 2009), gap junctional communication between astrocytes could provide better metabolic support to neurons than could be achieved by individual uncoupled astrocytes.

A role for gap junction-mediated astrocytic networks in the consolidation of wakefulness is further supported by the facts that astrocytic coupling changes depending on the vigilance state, increasing during wakefulness and decreasing during sleep (Petit and Magistretti, 2016), and that the wake-promoting drug, modafinil, used to treat narcolepsy, can significantly increase gap junctional coupling between cortical astrocytes (Liu et al., 2013).

Recently, lactate has also been identified as biomarker for sleep-wake cycles (Naylor et al., 2012). High resolution *in vivo* measurements of lactate in the brain via biosensors indicate that the analyte displays a daily variation with higher values during the active phase (Dash et al., 2013). Lactate also varies as a function of the sleep-wake cycle, increasing during wakefulness and decreasing during NREM sleep (Naylor et al., 2012; Dash et al., 2013; Wisor et al., 2013). Thus, our study provides direct evidence for the role of ANLS in wakefulness and remains in line with previous work showing that astrocyte-derived lactate is the preferred energy substrate for use by active neurons during awakening (Aubert et al.,

2005; Wyss et al., 2011; Sampol et al., 2013; Bouzier-Sore and Pellerin, 2013; Magistretti and Allaman, 2015).

Excessive sleepiness and an inability to maintain sustained episodes of wakefulness during the active phase are characteristics of human (Scammel et al., 2009) and animal models of narcolepsy (Lin et al., 1999; Chemelli et al., 1999; Willie et al., 2003; Mochizuki et al., 2004; Tabuchi et al., 2014). The main cause of narcolepsy is a marked and selective loss of orexin neurons in the LHA (Peyron et al., 2000; Thannickal et al., 2000). Although the sleep-wake phenotype observed in Cx43 cKO^{GFAP} mice is reminiscent of a narcolepsy-like phenotype, our video-EEG recordings did not show any of the two main other features of narcolepsy – cataplectic attacks and sudden intrusions of REM sleep during awakening (Scammel et al., 2009). Furthermore, the number of orexin neurons in the LHA remained normal in Cx43 cKO^{GFAP} mice. Narcolepsy without cataplexy can be considered as an early form of narcolepsy during which the frequency of cataplectic attacks progressively increases subsequent to orexin neuron degeneration (Baumann et al., 2014; Tabuchi et al., 2014).

In conclusion, we propose a hitherto unknown regulatory mechanism of sleep-wake cycle involving astrocyte-neuron metabolic interactions. Using EEG, in vitro electrophysiology and astrocytic-specific molecular genetics, we demonstrate that activity of orexin neurons depends on energy metabolites trafficking through astroglial metabolic networks, a mechanism that is critical for maintaining normal daily cycle of wakefulness. We also provide strong evidence of the importance of ANLS in this process.

Star Methods

Contact for reagent and resource sharing

Further information and requests for resources and reagents should be directed to and will be fulfilled by the Lead Contact, Philip Haydon (philip.haydon@tufts.edu).

Experimental model and subject details

Animals, housing and genotyping—Astrocyte-specific Cx43 conditional knockout (cKO) mice were generated with the Cre/LoxP system by breeding homozygous floxed Cx43 mice (Cx43$^{f/f}$; Liao et al., 2001) to human glial fibrillary acidic protein (hGFAP)-Cre mice (Casper and McCarthy, 2006), as previously reported (Wiencken-Barger et al., 2007; Han et al., 2014). Cx43$^{f/f}$ and hGFAP-Cre transgenic lines were obtained from Dr. Ken D. McCarthy (Department of Pharmacology, University of North Carolina, Chapel Hill, NC, USA). In Cx43$^{f/f}$ mice, Exon 2 of Cx43 allele was flanked by two LoxP sites, while in GFAP-Cre mice, a DNA fragment encoding Cre recombinase was inserted into an expression cassette containing a 2.2 kb human GFAP promoter, *gfa2*, to drive the expression of inducible Cre recombinase in GFAP-expressing cells. Homozygous floxed Cx43 mice and hGFAP-Cre mice were backcrossed for at least 10 generations to C57BL/6J mice before intercrossing. To generate experimental animals, homozygous floxed Cx43 Cre-positive mice (Cx43$^{f/f}$:hGFAP-Cre+ aka Cx43 cKO^{GFAP}) were bred to homozygous floxed Cre-negative mice (Cx43$^{f/f}$:hGFAP-Cre- aka Cx43$^{f/f}$). The resulting offspring were all homozygous floxed and either hemizygous or negative for hGFAP-Cre. The following

primers were used for PCR genotyping from tail DNA: for floxed Cx43 (WT band 400 bp; floxed band 450 bp) forward 5′-CTTTGACTCTGATTACAGAGCTTAA-3′ and reverse 5′-GTCTCACTGTTACTTAACAGCTTGA-3′; for hGFAP-Cre (500 bp band) forward 5′-GGTCGATGCAACGAGTGATGAGG-3′ and reverse 5′-GCTAAGTGCCTTCTCTACACCTGCG-3′. Littermates with homozygous floxed Cre-negative ($Cx43^{f/f}$) or WT mice with the same C57BL/6J genetic background were used as controls as specified in the results.

Mice were bred and housed on a 12/12 light/dark cycle (8 am/8 pm) and given standard chow and water ad libitum. These experiments were performed with the approval of the Institutional Animal Care and Use Committee of Tufts University and the Universities of Lille, and under the guidelines defined by the National Institutes of Health Guide for the Care and Use of Laboratory Animals and the the European Union Council Directive of September 22, 2010 (2010/63/EU).

Method details

Western blot analysis—Eight weeks old male mice were anesthetized with isoflurane prior to decapitation. Brains were rapidly removed from the skull and frozen at −80 °C until processed for protein extractions. Homogenates from whole-brain tissues were prepared as previously described (Brand-Schieber et al., 2005). Frozen brains were placed in lysis buffer (50 mM NaCl, 25 mM Tris–HCl, 5 mM EDTA, 1% NP-40, 0.25 mM Na-deoxycholate, pH 7.5) and tissue sonicated. Samples of whole-cell lysates in Laemmli buffer (20 μg total protein) were electrophoresed in 4–20% SDS-PAGE (Bio-Rad, Hercules, CA) and then transferred to nitrocellulose membranes (Schleicher & Schuell, Keene, NH, USA). Immunoblots were performed after overnight incubation of membranes with blocking solution (5% dry nonfat milk and 0.4% polyoxyethylenesorbitan monolaurate: Tween-20; Sigma) using the following primary antibodies: rabbit polyclonal anti-connexin43 (1:2000, Sigma) and mouse monoclonal anti-GAPDH (1:5000, Fitzgerald).

After several washes with 1X PBS-Tween-20, membranes were incubated with the following HRP-conjugated secondary antibodies: goat polyclonal anti-rabbit (1:2000, Santa Cruz Biotechnology, Santa Cruz, CA, USA) and goat polyclonal anti-mouse (1:2000, Santa Cruz Biotechnology, Santa Cruz, CA, USA). Detection of bands was performed on X-ray films (Kodak, Rochester, NY, USA) following incubation with enhanced chemiluminescence reagents (Amersham Pharmacia Biotechnology, Piscataway, NJ, USA).

EEG/EMG surgery, recording and analysis—Electroencephalogram (EEG)/electromyogram (EMG) implantation surgery was performed as previously described (Clasadonte et al., 2013; 2014). Eight weeks old male $Cx43^{f/f}$, Cx43 cKO^{GFAP} and WT mice were anaesthetized with isoflurane and placed into a stereotaxic frame. For implantation of EEG electrodes, skull surface was exposed, and four insulated wire electrodes (Cooner Wire) were placed and screwed as follows: two extradural cortical electrodes were inserted bilaterally in the frontal areas and the two others were inserted bilaterally in the parietal areas. For implantation of EMG, two insulated wire electrodes were inserted bilaterally into the nuchal muscle. Electrodes connected to a microconnector (Pinnacle Technology) were

secured at the surface of the skull with dental acrylic. After surgery, mice were intraperitoneally injected with buprenorphine (0.08 mg/kg) and lactated Ringer solution, fed with soaked rodent food. After 4 days of post-operative recovery, freely moving mice were placed into individual topless Plexiglas circle boxes (Pinnacle Technology) containing water and food ad libitum and their microconnectors plugged to a lightweight EEG preamplifier (Pinnacle Technology). Animals were acclimated for two days before data collection, monitored with video camera system (Pinnacle Technology) and maintained on a 8 am/8 pm light/dark cycle.

EEG and EMG signals were band-pass filtered at 1–100 Hz, digitized at 200 Hz, and acquired with a computer-based system and Sirenia software (Pinnacle Technology). Sleep stages were scored visually based on 4 s epochs by a trained experimenter using SleepSign for Animal software (Kissei Comtec). Wakefulness (W) consisted of low-amplitude, high frequency EEG and high EMG activity; rapid eye movement (REM) sleep consisted of low-amplitude, desynchronized EEG with low EMG activity; and non-rapid eye movement (NREM) sleep consisted of high-amplitude, low frequency EEG with little EMG modulation. Brief awakenings defined as uninterrupted waking episodes of 1–4 s epochs were not included in the analysis. Epochs containing movement artifacts were included in the state totals. After assignments of state scores, the amount of each state (expressed as a percentage of the total recording time in 1 hour time bins) and their duration were measured.

Adeno-associated virus vector—To selectively delete Cx43 from LHA astrocytes in $Cx43^{f/f}$ mice, we produced a recombinant AAV expression plasmid by placing a Cre:GFP fusion protein (Addgene, Cambridge, MA; Matsuda and Cepko, 2007) under control of the astrocyte-specific human GFAP promoter, hGfa2 (Addgene, Cambridge, MA; Brenner et al., 1994; Lee et al., 2008). AAV constructs also contained a 3′ woodchuck hepatitis virus posttranscriptional regulatory element (WPRE) to induce expression of intronless viral messages and increase the stability and level of gene expression (Martin et al., 2002). Recombinant AAV8 was packaged in cultures of HEK 293T cells. Approximately 1.5×10^7 293T cells were seeded into 150 cm dishes in complete DMEM supplemented with 10% fetal bovine serum, 1 mM MEM sodium pyruvate, 0.1 mM MEM nonessential amino acids solution, and 0.05% Penicillin-Streptomycin (5,000 units/mL). At 24 h media was changed to culture media containing 5% FBS and cells were transfected three separate plasmids: 1) Adeno helper plasmid (pFΔ6), 2) AAV helper encoding the Rep 2 and Cap 8 sequences for serotype 8 (pAR8; Broekman et al., 2006), and 3) the recombinant Cre:GFP expression plasmid described above. After culturing cells for 48 h at 37° C, 5% CO_2, cells were harvested and pelleted by centrifugation. The pellet was resuspended in 10 mM Tris, pH 8.0 and chilled on ice. Cells were lysed by repeated freeze-thaw cycles followed by treatment with 50 U benzonase (Novagen, CA) and 0.5% sodium deoxycholate for 30 min at 37° C. Virus was purified by density gradient centrifugation in iodixinol (Zolotukhin et al., 1999). Two buffer exchanges with ACSF were performed. The purified virus was then concentrated in ACSF by centrifugation in Amicon Ultra-15 Centrifugal Filter Units. The final preparation was sterile filtered through a milipore syringe filter. The titer of each virus (2.1×10^{12} virus genomes per mL) was determined by quantitative RT-PCR using primers and a probe specific for the WPRE sequence.

Stereotaxic virus injection—Eight weeks old male $Cx43^{f/f}$ mice were anesthetized with isoflurane, placed into a stereotaxic frame and two small holes were bilaterally opened in the skull. A 2 μL Neuro 7002 syringe (Hamilton) was filled with AAV (1×10^9 virus genomes per μL) and the needle inserted into the lateral hypothalamic area (LHA; coordinate AP/DV/ML = −1.6/−5.35/±0.9 mm). One μL of vector per hemisphere was injected with pressure at a speed of 0.10 μL/min using a Microsyringe Pump Controller Micro4 (World Precision Instruments). For controls, AAV and artificial cerebrospinal fluid (ACSF) were injected into the LHA of WT and $Cx43^{f/f}$ mice, respectively. Mice were allowed to recover for 10 days before the implantation of EEG/EMG electrodes, as described earlier.

Virus and drug injections in freely behaving mice—Eight week old male $Cx43^{f/f}$ mice were anesthetized with isoflurane, placed into a stereotaxic frame and two small holes were bilaterally opened in the skull. Bilateral brain cannula was stereotaxically implanted into the LHA (coordinate AP/DV/ML = −1.6/−5.35/±0.9 mm). Mice were then implanted with EEG/EMG electrodes, as described earlier. After 4 days of post-operative recovery, freely moving mice were placed into individual topless Plexiglas circle boxes and their microconnectors plugged to EEG preamplifier, as described earlier. One week after surgery, 1 μL of vector per hemisphere was injected into the LHA of freely behaving mice through the bilateral cannula with pressure at a speed of 0.10 μL/min using a Microsyringe Pump Controller Micro4 (World Precision Instruments).

Osmotic mini-pumps (model 1002; Alzet; flow rate, 0.25 μL/h; 2-wk duration) were filled with sodium L-lactate (5 mM in ACSF; Alfa Aesar) or vehicle (ACSF for control injection), secured with the flow moderator, and primed overnight in 0.9% saline solution at 37 °C before to be connected to the bra in cannula by flexible catheter tubing. Osmotic mini-pumps were externalized as previously described (Clasadonte et al., 2013). Briefly, they were placed in a sealed conic tube of 1 mL filled with 0.9% saline solution, and maintained at 37 °C with a iBlock Mini Dry Bath (Midsci) placed out of the cage. The catheter tubing was filled with lactate (5 mM in ACSF; Alfa Aesar) or vehicle (ACSF for control injection). A small air bubble was inserted into the catheter tubing during its connection with the pump to monitor the flow rate estimated at 0.25 μL/h in our conditions. The flexible catheter tubing was carefully aligned and attached to the EEG cable. The presence of a swivel (Pinnacle Technology) prevented the torsion of tubing and cable. ACSF control injection was performed 21 days after the virus injection. One week later, catheter tubing and mini-pumps filled with ACSF and connected to the bilateral cannula were removed and replaced with catheter tubing and mini-pumps filled with sodium L-lactate (5 mM in ACSF; Alfa Aesar). Lactate infusion lasted for one week.

Immunohistochemistry—To map the AAV-hGfa2-Cre:GFP injection sites and cell targeting specificity, brain sections were immunostained after completion of the experiments. Mice were deeply anesthetized with a mixture of ketamine hydrochloride and xylazine hydrochloride. They were perfused sequentially via the left ventricle with 20 mL chilled phosphate buffer saline (PBS) solution (1x) and 100 mL 4% paraformaldehyde in PBS solution (1x, pH 7.4). Brains were removed and postfixed in the same fixative for 24 h at 4 °C. After fixation, they were soaked 24 h in a solution of 30% sucrose. Coronal sections

containing the LHA were cut serially at 200-μm intervals on a freezing microtome (SM2000R; Leica) into at a thickness of 40 μm and then stored in an antifreeze solution at −20 °C until immunostaining. For determining cell targeting specificity of AAV, double-immunostaining GFAP/orexin-A or GFAP/neuronal nuclei (NeuN) was conducted on free-floating sections incubated with 5% normal goat serum (NGS) blocking solution for 1 h at room temperature and then with primary antibodies overnight at 4 °C on a shaking platform. The chicken anti-GFA P antibody (1:1000; Abcam) was combined with either the rabbit anti-orexin-A antibody (1:1000; Millipore) or the mouse anti-NeuN antibody (1:1000; Millipore). Sections were rinsed three times with 1x PBS solution and then incubated with secondary antibodies for 2 h at room temperature. The following secondary antibodies were used: goat anti-chicken Alexa Fluor 633 (1:1000; Invitrogen) with goat anti-rabbit Alexa Fluor 546 (1:1000; Invitrogen) or goat anti-chicken Alexa Fluor 633 (1:1000; Invitrogen) with goat anti-mouse Alexa Fluor 546 (1:1000; Invitrogen). All sections were counterstained with DAPI, mounted on slides and coverslipped with Vectashield antifade mounting medium. Due to GFP expression, the site of AAV injection was clearly observable using an epifluorescence microscope (Keyence BZ-X700). Entire sections were automatically imaged with a 10x objective and stitched with Keyence software. To examine cell targeting specificity, fluorescent images were acquired with a confocal laser scanning microscope (Nikon A1) using a 40x objective. Image analysis and counting of cells expressing GFP alone, GFP with GFAP, GFP with orexin-A and GFP with NeuN were performed within an area of interest in the LHA by using Fiji software.

To determine the number of orexin neurons in $Cx43^{f/f}$ and Cx43 cKO^{GFAP} mice that were not transduced with AAV, the same immunohistochemical procedure as stated above was followed by using the rabbit anti-orexin-A primary antibody (1:1000; Millipore) and the goat anti-rabbit Alexa Fluor 546 secondary antibody (1:1000; Invitrogen). Fluorescent images were acquired with a confocal laser scanning microscope (Nikon A1) using a 20x objective. Orexin-A-immunopositive cells were bilaterally counted in a square region (634.88 μm x 634.88 μm) within the LHA in all the sections that had fluorescent cell bodies by using Fiji software.

Brain slice preparation—Eight weeks old male $Cx43^{f/f}$ and Cx43 cKO^{GFAP} mice were anaesthetized with isoflurane, and after decapitation, the brain was rapidly removed and put in ice-cold oxygenated (O_2 95%/CO_2 5%) artificial cerebrospinal fluid (ACSF) containing the following (in mM): 120 NaCl, 3.2 KCl, 1 NaH_2PO_4, 26 $NaHCO_3$, 1 $MgCl_2$, 2 $CaCl_2$, 2.5 glucose (osmolarity adjusted to 300 mOsm with sucrose, pH 7.4). After removal of the cerebellum, the brain was glued and coronal hypothalamic slices containing the LHA were cut using a vibratome (VT1200S; Leica). Before recording, slices were incubated at 35°C for a recovery period of 1 h. After recovery, slices were placed in a submerged recording chamber (31°C; Warner Instruments) and continuously perfused (2 ml/min) with oxygenated ACSF. The glucose concentration used for recordings was 2.5 mM unless otherwise stated.

All drugs were applied to the perfusing system (bath application) to obtain the final concentrations indicated unless otherwise stated. Alpha-cyano-4-hydroxycinnamic acid (4-CIN), carbenoxolone disodium salt, sodium oxamate, sodium pyruvate, and tolbutamide

were obtained from Sigma, sodium L-lactate from Alfa Aesar and tetrodotoxin citrate (TTX) from Tocris.

Patch-clamp recordings—Neurons and astrocytes located in the LHA were visually identified with a 16x objective and 2x magnification in an upright Nikon Eclipse FN1 microscope or with a 40x magnification in an upright Leica DM-LFSA microscope by using infrared differential interference contrast (IR-DIC). Whole-cell patch-clamp recordings were performed in current- and voltage-clamp modes by using a Multiclamp 700B amplifier (Molecular Devices). Data were filtered at 1 kHz and sampled at 5 kHz with Digidata 1322A interface and Clampex 9.2 and 10.6 from pClamp software (Molecular Devices). Pipettes (from borosilicate capillaries; World Precision Instruments) had resistance of 6–8 MΩ when filled with an internal solution containing the following (in mM): 123 K-gluconate, 2 $MgCl_2$, 8 KCl, 0.2 EGTA, 4 Na_2-ATP, 0.3 Na-GTP, and 10 HEPES, pH 7.3 with KOH. Biocytin (2 mg/mL; Sigma) was also added to the internal solution for post-hoc immunohistochemical phenotyping and evaluation of gap junctional coupling. For this latter, recordings were realized in current-clamp mode and limited to exactly 20 min. In some experiments, sodium L-lactate (2.5 or 5 mM; Alfa Aesar) was added to the internal solution. Loose patch-clamp recordings were performed in neurons in current-clamp mode and whole-cell configuration was achieved at the end of the experiment for electrophysiological and immunohistochemical characterization. All recordings were analyzed with Clampfit 9.2 and 10.6 from pClamp software (Molecular Devices). Instantaneous action potential firing was calculated as the inverse of each action potential interval. Junction potentials were determined to allow correction of membrane potential values. Orexin neurons exhibited tonic spontaneous firing (Figure 2A1), a H-current, a monophasic after hyperpolarizing potential and a low-threshold spike in response to 1 s negative and positive current pulses (from − 80 pA to 70 pA in 10 pA increments; Figures 4B and S2A). These electrophysiological membrane properties were different from those of melanin-concentratin hormone neurons residing in the same region (Eggermann et al., 2003; Parsons and Hirasawa, 2010). Electrical membrane properties of astrocytes was measured in voltage-clamp mode by applying a series voltage pulses from − 100 mV to + 100 mV (300 ms, 10 mV increments) from a holding potential of − 80 mV. Input resistance (R_{in}) was determined by measuring the slope of the linear portion of the current-voltage (I–V) curve. Astrocytes in the LHA showed typical glial cell membrane properties (Steinhauser, 1993; Sontheimer, 1994) characterized by the lack of action potential firing in response to depolarizing current steps (Figure 4B), a linear current-voltage (I–V) relationship (Figures S4A1 and S4A2), a very negative RMP (−85.70±1.05 mV; n=17 cells from 5 animals; Figure S4C), and a low Rin (42.81±6.70 MΩ; n=17 cells from 5 animals; Figure S4D).

For glucose diffusion experiments, the internal solution contained the fluorescent glucose derivative 2-[N-(7-nitrobenz-2-oxa-1,3-diazol-4-yl)amino]-2-deoxyglucose (2-NBDG; 2 mg/ml; Invitrogen) and dextran tetramethylrhodamine (1 mg/ml; Molecular Probes). Recorded cells were loaded with these molecules during 20 minutes in current-clamp mode. Intercellular diffusion of fluorescent molecules was captured online with a digital camera exactly after 20 min and the number of coupled cells was analyzed offline with Fiji software.

For paired astrocyte-neuron whole-cell current-clamp recordings, one astrocyte was first recorded and filled with the gap junction-permeable tracer, Lucifer yellow CH dilithium salt (1 mg/ml; Sigma) through the patch pipette. Twenty min after basal astrocyte recording, one distant orexin neuron (intercellular distance of 50–75 μm) was recorded and filled with the membrane-impermeable dye, Alexa Fluor 594 hydrazide (40 μM; Invitrogen) through the patch pipette.

Cell phenotyping and dye-coupling analysis—Immediately after electrophysiological recordings, slices were fixed overnight with 4% paraformaldehyde in PBS solution (1x, pH 7.4) at 4 °C and then rinsed several times with PBS solution and permeabilized and immunoblocked with 0.5% Triton X-100 and 5% NGS in PBS for 30 min at room temperature. For immunohistochemical phenotyping of recorded neurons filled with biocytin, slices were incubated with the rabbit anti-orexin-A primary antibody (1:1000; Millipore) in Triton/NGS/PBS for 3 days at 4°C. After several washes in 1x PBS solution, slices were incubated with the goat anti-rabbit Alexa Fluor 488 secondary antibody (1:500; Invitrogen) and streptavidin Alexa Fluor 546 (1:250; Invitrogen) in Triton/NGS/PBS overnight at 4°C. In some experiments, biocytin revelation was combined with double-immunolabeling for GFAP and NeuN to determine the phenotype of the coupled cells. To this end, slices were incubated with primary antibodies chicken anti-GFAP (1:1000; Abcam) and mouse anti-NeuN (1:1000; Millipore) in Triton/NGS/PBS for 3 days at 4°C and then treated with secondary antibodies goat anti-chicken Alexa Fluor 633 (1:500; Invitrogen) and goat anti-mouse Alexa Fluor 546 (1:500; Invitrogen) and streptavidin Alexa Fluor 488 (1:250; Invitrogen) in Triton/NGS/PBS overnight at 4°C. After several washes in 1x PBS solution, slices were mounted on slides and coverslipped with Vectashield antifade mounting medium. Fluorescent images were acquired with a confocal laser scanning microscope (Nikon A1). To determine the number of coupled cells, stack of optical sections at 3 μm intervals through the depth of the slice were obtained and images were analyzed by using Fiji software.

Quantification and statistical analysis

SigmaPlot 11 and 13 from Systat software was used to perform all statistical analysis. The difference between several groups was analyzed by one-way ANOVA. Two-way ANOVA was used when more than two comparisons (with time and genotype) were made. Repeated-measures ANOVAs were used when multiple measurements were made over time in the same groups. ANOVA was followed by the Student–Newman–Keuls or the nonparametric Dunn's post-hoc multiple comparisons tests. Comparisons between two groups were conducted with the paired or unpaired Student t-test or the nonparametric Mann–Whitney test as appropriate. The level of significance was set at $p<0.05$. Data are presented as mean ± SEM.

Supplementary Material

Refer to Web version on PubMed Central for supplementary material.

Acknowledgments

P.G.H. was supported by NIH grants, J.C by the Epilepsy Foundation, Marie Skłodowska-Curie Actions – European Research Fellowship (H2020-MSCA-IF-2014, ID656657) and Région Hauts-de-France (program VisionAIRR), E.S. by NIH/NINDS (R01NS092466 and R01NS092786) and D.B. by the NINDS (R01 NS084920). The authors declare that P.G.H. has equity interest in GliaCure Inc.

References

Adamantidis AR, Zhang F, Aravanis AM, Deisseroth K, de Lecea L. Neural substrates of awakening probed with optogenetic control of hypocretin neurons. Nature. 2007; 450:420–4. [PubMed: 17943086]

Araque A, Carmignoto G, Haydon PG, Oliet SH, Robitaille R, Volterra A. Gliotransmitters travel in time and space. Neuron. 2014; 81:728–39. [PubMed: 24559669]

Aubert A, Costalat R, Magistretti PJ, Pellerin L. Brain lactate kinetics: Modeling evidence for neuronal lactate uptake upon activation. Proc Natl Acad Sci U S A. 2005; 102:16448–53. [PubMed: 16260743]

Ball KK, Gandhi GK, Thrash J, Cruz NF, Dienel GA. Astrocytic connexin distributions and rapid, extensive dye transfer via gap junctions in the inferior colliculus: implications for [(14)C]glucose metabolite trafficking. J Neurosci Res. 2007; 85:3267–3283. [PubMed: 17600824]

Baumann CR, Mignot E, Lammers GJ, Overeem S, Arnulf I, Rye D, Dauvilliers Y, Honda M, Owens JA, Plazzi G, et al. Challenges in diagnosing narcolepsy without cataplexy: a consensus statement. Sleep. 2014; 37:1035–42. [PubMed: 24882898]

Bélanger M, Allaman I, Magistretti PJ. Brain energy metabolism: focus on astrocyte-neuron metabolic cooperation. Cell Metab. 2011; 14:724–38. [PubMed: 22152301]

Bouzier-Sore AK, Pellerin L. Unraveling the complex metabolic nature of astrocytes. Front Cell Neurosci. 2013; 7:179. [PubMed: 24130515]

Brand-Schieber E, Werner P, Iacobas DA, Iacobas S, Beelitz M, Lowery SL, Spray DC, Scemes E. Connexin43, the major gap junction protein of astrocytes, is down-regulated in inflamed white matter in an animal model of multiple sclerosis. J Neurosci Res. 2005; 80:798–808. [PubMed: 15898103]

Brenner M, Kisseberth WC, Su Y, Besnard F, Messing A. GFAP promoter directs astrocyte-specific expression in transgenic mice. J Neurosci. 1994; 14:1030–7. [PubMed: 8120611]

Broekman ML, Comer LA, Hyman BT, Sena-Esteves M. Adeno-associated virus vectors serotyped with AAV8 capsid are more efficient than AAV-1 or -2 serotypes for widespread gene delivery to the neonatal mouse brain. Neuroscience. 2006; 138:501–10. [PubMed: 16414198]

Brown RE, Basheer R, McKenna JT, Strecker RE, McCarley RW. Control of sleep and wakefulness. Physiol Rev. 2012; 92:1087–187. [PubMed: 22811426]

Bushong EA, Martone ME, Jones YZ, Ellisman MH. Protoplasmic astrocytes in CA1 stratum radiatum occupy separate anatomical domains. J Neurosci. 2002; 22(1):183–92. [PubMed: 11756501]

Casper KB, McCarthy KD. GFAP-positive progenitor cells produce neurons and oligodendrocytes throughout the CNS. Mol Cell Neurosci. 2006; 31:676–84. [PubMed: 16458536]

Chemelli RM, Willie JT, Sinton CM, Elmquist JK, Scammell T, Lee C, Richardson JA, Williams SC, Xiong Y, Kisanuki Y, et al. Narcolepsy in orexin knockout mice: molecular genetics of sleep regulation. Cell. 1999; 98:437–51. [PubMed: 10481909]

Clasadonte J, Dong J, Hines DJ, Haydon PG. Astrocyte control of synaptic NMDA receptors contributes to the progressive development of temporal lobe epilepsy. Proc Natl Acad Sci U S A. 2013; 110:17540–5. [PubMed: 24101472]

Clasadonte J, McIver SR, Schmitt LI, Halassa MM, Haydon PG. Chronic sleep restriction disrupts sleep homeostasis and behavioral sensitivity to alcohol by reducing the extracellular accumulation of adenosine. J Neurosci. 2014; 34:1879–91. [PubMed: 24478367]

Cruz NF, Ball KK, Dienel GA. Functional imaging of focal brain activation in conscious rats: impact of [(14)C]glucose metabolite spreading and release. J Neurosci Res. 2007; 85:3254–3266. [PubMed: 17265468]

Dash MB, Bellesi M, Tononi G, Cirelli C. Sleep/wake dependent changes in cortical glucose concentrations. J Neurochem. 2013; 124:79–89. [PubMed: 23106535]

De Pina-Benabou MH, Srinivas M, Spray DC, Scemes E. Calmodulin kinase pathway mediates the K^+-induced increase in Gap junctional communication between mouse spinal cord astrocytes. J Neurosci. 2001; 21:6635–6643. [PubMed: 11517253]

Eggermann E, Bayer L, Serafin M, Saint-Mleux B, Bernheim L, Machard D, Jones BE, Mühlethaler M. The wake-promoting hypocretin-orexin neurons are in an intrinsic state of membrane depolarization. J Neurosci. 2003; 23:1557–62. [PubMed: 12629156]

Gandhi GK, Cruz NF, Ball KK, Dienel GA. Astrocytes are poised for lactate trafficking and release from activated brain and for supply of glucose to neurons. J Neurochem. 2009; 111(2):522–36. [PubMed: 19682206]

Giaume C, Koulakoff A, Roux L, Holcman D, Rouach N. Astroglial networks: a step further in neuroglial and gliovascular interactions. Nat Rev Neurosci. 2010; 11:87–99. [PubMed: 20087359]

Giaume C, Theis M. Pharmacological and genetic approaches to study connexin-mediated channels in glial cells of the central nervous system. Brain Res Rev. 2010; 63:160–76. [PubMed: 19963007]

Goodenough DA, Goliger JA, Paul DL. Connexins, connexons, and intercellular communication. Annu Rev Biochem. 1996; 65:475–502. [PubMed: 8811187]

Halassa MM, Fellin T, Takano H, Dong JH, Haydon PG. Synaptic islands defined by the territory of a single astrocyte. J Neurosci. 2007; 27(24):6473–7. [PubMed: 17567808]

Halassa MM, Florian C, Fellin T, Munoz JR, Lee SY, Abel T, Haydon PG, Frank MG. Astrocytic modulation of sleep homeostasis and cognitive consequences of sleep loss. Neuron. 2009; 61:213–9. [PubMed: 19186164]

Halestrap AP, Price NT. The proton-linked monocarboxylate transporter (MCT) family: structure, function and regulation. Biochem J. 1999; 343(Pt 2):281–99. [PubMed: 10510291]

Han Y, Yu HX, Sun ML, Wang Y, Xi W, Yu YQ. Astrocyte-restricted disruption of connexin-43 impairs neuronal plasticity in mouse barrel cortex. Eur J Neurosci. 2014; 39:35–45. [PubMed: 24148096]

Hassani OK, Lee MG, Jones BE. Melanin-concentrating hormone neurons discharge in a reciprocal manner to orexin neurons across the sleep-wake cycle. Proc Natl Acad Sci U S A. 2009; 106:2418–22. [PubMed: 19188611]

Karagiannis A, Sylantyev S, Hadjihambi A, Hosford PS, Kasparov S, Gourine AV. Hemichannel-mediated release of lactate. J Cereb Blood Flow Metab. 2015; 36(7):1202–11. [PubMed: 26661210]

Kiyashchenko LI, Mileykovskiy BY, Maidment N, Lam HA, Wu MF, John J, Peever J, Siegel JM. Release of hypocretin (orexin) during waking and sleep states. J Neurosci. 2002; 22:5282–6. [PubMed: 12097478]

Lam TK, Gutierrez-Juarez R, Pocai A, Rossetti L. Regulation of blood glucose by hypothalamic pyruvate metabolism. Science. 2005; 309:943–7. [PubMed: 16081739]

Lee MG, Hassani OK, Jones BE. Discharge of identified orexin/hypocretin neurons across the sleep-waking cycle. J Neurosci. 2005; 25:6716–20. [PubMed: 16014733]

Lee Y, Messing A, Su M, Brenner M. GFAP promoter elements required for region-specific and astrocyte-specific expression. Glia. 2008; 56:481–93. [PubMed: 18240313]

Liao Y, Day KH, Damon DN, Duling BR. Endothelial cell-specific knockout of connexin 43 causes hypotension and bradycardia in mice. Proc Natl Acad Sci U S A. 2001; 98:9989–94. [PubMed: 11481448]

Lin L, Faraco J, Li R, Kadotani H, Rogers W, Lin X, Qiu X, de Jong PJ, Nishino S, Mignot E. The sleep disorder canine narcolepsy is caused by a mutation in the hypocretin (orexin) receptor 2 gene. Cell. 1999; 98:365–76. [PubMed: 10458611]

Liu X, Petit JM, Ezan P, Gyger J, Magistretti P, Giaume C. The psychostimulant modafinil enhances gap junctional communication in cortical astrocytes. Neuropharmacology. 2013; 75:533–8. [PubMed: 23665355]

Magistretti PJ, Allaman I. A cellular perspective on brain energy metabolism and functional imaging. Neuron. 2015; 86:883–901. [PubMed: 25996133]

Martin KR, Klein RL, Quigley HA. Gene delivery to the eye using adeno-associated viral vectors. Methods. 2002; 28:267–75. [PubMed: 12413426]

Matsuda T, Cepko CL. Controlled expression of transgenes introduced by in vivo electroporation. Proc Natl Acad Sci U S A. 2007; 104:1027–32. [PubMed: 17209010]

Mileykovskiy BY, Kiyashchenko LI, Siegel JM. Behavioral correlates of activity in identified hypocretin/orexin neurons. Neuron. 2005; 46:787–98. [PubMed: 15924864]

Mochizuki T, Crocker A, McCormack S, Yanagisawa M, Sakurai T, Scammell TE. Behavioral state instability in orexin knock-out mice. J Neurosci. 2004; 24:6291–300. [PubMed: 15254084]

Nagy JI, Rash JE. Connexins and gap junctions of astrocytes and oligodendrocytes in the CNS. Brain Res Brain Res Rev. 2000; 32:29–44. [PubMed: 10751655]

Naylor E, Aillon DV, Barrett BS, Wilson GS, Johnson DA, Johnson DA, Harmon HP, Gabbert S, Petillo PA. Lactate as a biomarker for sleep. Sleep. 2012; 35:1209–22. [PubMed: 22942499]

Oliveira JF, Sardinha VM, Guerra-Gomes S, Araque A, Sousa N. Do stars govern our actions? Astrocyte involvement in rodent behavior. Trends Neurosci. 2015; 38:535–49. [PubMed: 26316036]

Pannasch U, Rouach N. Emerging role for astroglial networks in information processing: from synapse to behavior. Trends Neurosci. 2013; 36:405–17. [PubMed: 23659852]

Parsons MP, Hirasawa M. ATP-sensitive potassium channel-mediated lactate effect on orexin neurons: implications for brain energetics during arousal. J Neurosci. 2010; 30:8061–70. [PubMed: 20554857]

Paukert M, Agarwal A, Cha J, Doze VA, Kang JU, Bergles DE. Norepinephrine controls astroglial responsiveness to local circuit activity. Neuron. 2014; 82:1263–70. [PubMed: 24945771]

Pellerin L, Magistretti PJ. Glutamate uptake into astrocytes stimulates aerobic glycolysis: a mechanism coupling neuronal activity to glucose utilization. Proc Natl Acad Sci U S A. 1994; 91:10625–9. [PubMed: 7938003]

Petit JM, Magistretti PJ. Regulation of neuron-astrocyte metabolic coupling across the sleep-wake cycle. Neuroscience. 2016; 323:135–56. [PubMed: 26704637]

Peyron C, Faraco J, Rogers W, Ripley B, Overeem S, Charnay Y, Nevsimalova S, Aldrich M, Reynolds D, Albin R, et al. A mutation in a case of early onset narcolepsy and a generalized absence of hypocretin peptides in human narcoleptic brains. Nat Med. 2000; 6:991–7. [PubMed: 10973318]

Rouach N, Koulakoff A, Abudara V, Willecke K, Giaume C. Astroglial metabolic networks sustain hippocampal synaptic transmission. Science. 2008; 322:1551–5. [PubMed: 19056987]

Sada N, Lee S, Katsu T, Otsuki T, Inoue T. Epilepsy treatment. Targeting LDH enzymes with a stiripentol analog to treat epilepsy. Science. 2015; 347:1362–7. [PubMed: 25792327]

Sakurai T. The neural circuit of orexin (hypocretin): maintaining sleep and wakefulness. Nat Rev Neurosci. 2007; 8:171–81. [PubMed: 17299454]

Sampol D, Ostrofet E, Jobin ML, Raffard G, Sanchez S, Bouchaud V, Franconi JM, Bonvento G, Bouzier-Sore AK. Glucose and lactate metabolism in the awake and stimulated rat: a (13)C-NMR study. Front Neuroenergetics. 2013; 5:5. [PubMed: 23755012]

Scammell TE, Willie JT, Guilleminault C, Siegel JM. International Working Group on Rodent Models of Narcolepsy. A consensus definition of cataplexy in mouse models of narcolepsy. Sleep. 2009; 32:111–6. [PubMed: 19189786]

Schindelin J, Arganda-Carreras I, Frise E, Kaynig V, Longair M, Pietzsch T, Preibisch S, Rueden C, Saalfeld S, Schmid B, et al. Fiji: an open-source platform for biological-image analysis. Nat Methods. 2012; 9:676–682. [PubMed: 22743772]

Sontheimer H. Voltage-dependent ion channels in glial cells. Glia. 1994; 11:156–72. [PubMed: 7523291]

Stehberg J, Moraga-Amaro R, Salazar C, Becerra A, Echeverría C, Orellana JA, Bultynck G, Ponsaerts R, Leybaert L, Simon F, et al. Release of gliotransmitters through astroglial connexin 43 hemichannels is necessary for fear memory consolidation in the basolateral amygdala. FASEB J. 2012; 26(9):3649–57. [PubMed: 22665389]

Steinhäuser C. Electrophysiologic characteristics of glial cells. Hippocampus. 1993; 3:113–23.

Tabuchi S, Tsunematsu T, Black SW, Tominaga M, Maruyama M, Takagi K, Minokoshi Y, Sakurai T, Kilduff TS, Yamanaka A. Conditional ablation of orexin/hypocretin neurons: a new mouse model for the study of narcolepsy and orexin system function. J Neurosci. 2014; 34:6495–509. [PubMed: 24806676]

Tang F, Lane S, Korsak A, Paton JF, Gourine AV, Kasparov S, Teschemacher AG. Lactate-mediated glia-neuronal signalling in the mammalian brain. Nat Commun. 2014; 5:3284. [PubMed: 24518663]

Thannickal TC, Moore RY, Nienhuis R, Ramanathan L, Gulyani S, Aldrich M, Cornford M, Siegel JM. Reduced number of hypocretin neurons in human narcolepsy. Neuron. 2000; 27:469–74. [PubMed: 11055430]

Theis M, Jauch R, Zhuo L, Speidel D, Wallraff A, Döring B, Frisch C, Söhl G, Teubner B, Euwens C, et al. Accelerated hippocampal spreading depression and enhanced locomotory activity in mice with astrocyte-directed inactivation of connexin43. J Neurosci. 2003; 23:766–76. [PubMed: 12574405]

Tsunematsu T, Kilduff TS, Boyden ES, Takahashi S, Tominaga M, Yamanaka A. Acute optogenetic silencing of orexin/hypocretin neurons induces slow-wave sleep in mice. J Neurosci. 2011; 31:10529–39. [PubMed: 21775598]

Wiencken-Barger AE, Djukic B, Casper KB, McCarthy KD. A role for Connexin43 during neurodevelopment. Glia. 2007; 55:675–86. [PubMed: 17311295]

Willie JT, Chemelli RM, Sinton CM, Tokita S, Williams SC, Kisanuki YY, Marcus JN, Lee C, Elmquist JK, Kohlmeier KA, et al. Distinct narcolepsy syndromes in Orexin receptor-2 and Orexin null mice: molecular genetic dissection of Non-REM and REM sleep regulatory processes. Neuron. 2003; 38:715–30. [PubMed: 12797957]

Wisor JP, Rempe MJ, Schmidt MA, Moore ME, Clegern WC. Sleep slow-wave activity regulates cerebral glycolytic metabolism. Cereb Cortex. 2013; 23:1978–1987. [PubMed: 22767634]

Wyss MT, Jolivet R, Buck A, Magistretti PJ, Weber B. In vivo evidence for lactate as a neuronal energy source. J Neurosci. 2011; 31:7477. [PubMed: 21593331]

Zolotukhin S, Byrne BJ, Mason E, Zolotukhin I, Potter M, Chesnut K, Summerford C, Samulski RJ, Muzyczka N. Recombinant adeno-associated virus purification using novel methods improves infectious titer and yield. Gene Ther. 1999; 6:973–85. [PubMed: 10455399]

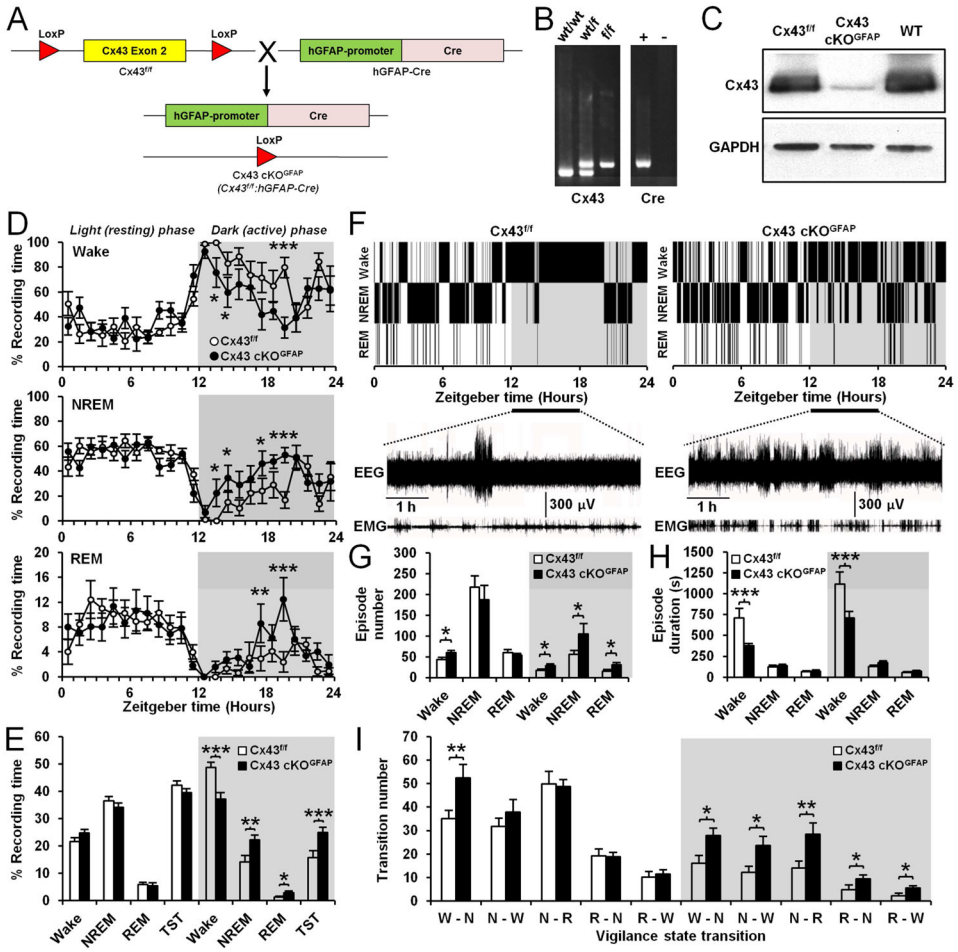

Figure 1. Deletion of Cx43 in astrocytes causes sleepiness and wakefulness instability during active phase

(A) Generation of mice with conditional knockout of Cx43 in astrocytes. (B) Left panel: Genotype PCR for the floxed Cx43 allele in wild-type (WT; wt/wt), heterozygous (wt/f) and homozygous (f/f) floxed mice. Right panel: Genotype PCR for GFAP-Cre in Cre-positive mice (+) and Cre-negative littermates (−). (C) Western blot showing Cx43 expression in whole-brain lysates from $Cx43^{f/f}$, Cx43 cKO^{GFAP} and WT mice. (D) Percentage average of the time spent in wake (top), NREM sleep (middle) and REM sleep (bottom) per h in $Cx43^{f/f}$ (n=8) and Cx43 cKO^{GFAP} mice (n=7; Wake, NREM and REM sleep: ANOVA followed by post-hoc test, *p<0.05, **p<0.01 and ***p<0.001). (E) Averaged percentage of time spent in wake, NREM and REM sleep during the 12h light phase and 12h dark phase in $Cx43^{f/f}$ (n=8) and Cx43 cKO^{GFAP} mice (n=7, ANOVA followed by post-hoc test, *p<0.05, **p<0.01 and ***p<001). TST: Total sleep time including REM and NREM sleep. (F) Representative hypnograms of $Cx43^{f/f}$ (left) and Cx43 cKO^{GFAP} mice (right). Bottom traces represent EEG/EMG recordings from ZT12 to ZT18. (G and H) Averages of the number (G) and duration (H) of wake, NREM and REM sleep episodes during the 12h light and dark phases in $Cx43^{f/f}$ (n=8) and Cx43 cKO^{GFAP} mice (n=7; ANOVA followed by post-hoc test, *p<0.05 and ***p<0.001). (I) Average number of transitions between vigilance states (W:

Wake, N: NREM, R: REM) in $Cx43^{f/f}$ (n=8) and Cx43 cKO^{GFAP} mice (n=7; ANOVA followed by post-hoc test, *p<0.05 and **p<0.01). See also Figure S1.

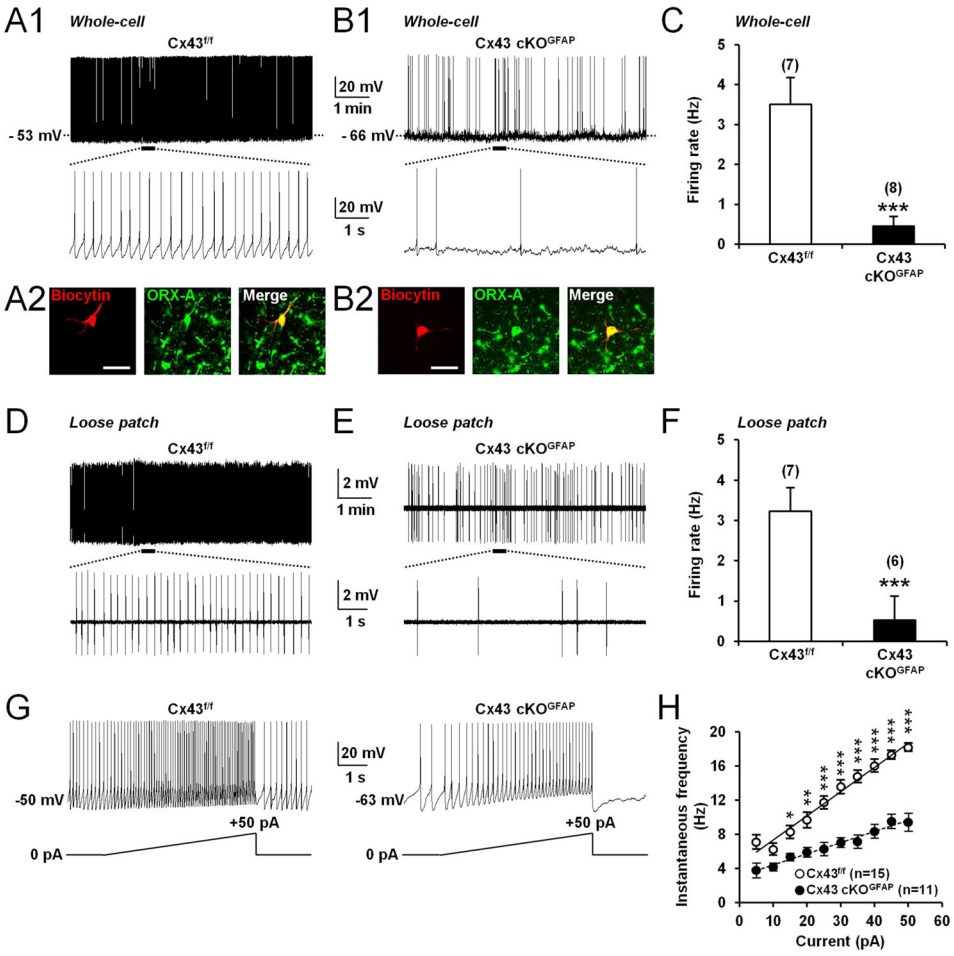

Figure 2. Deletion of Cx43 in astrocytes decreases spontaneous firing frequency and excitability of orexin neurons

(A1) Whole-cell current-clamp recording performed in ACSF containing 2.5mM glucose showing spontaneous tonic firing in an orexin neuron from Cx43$^{f/f}$ mouse. The bottom trace shows an expanded time scale of that recording. (A2) Images showing the cell recorded in (A1) filled with biocytin (red) and expression of orexin (ORX)-A (green). Scale bar: 50μm. (B1 and B2) Same experiments as in (A1 and B1) but in an orexin neuron from Cx43 cKO^{GFAP} mouse. (C) Average firing rate of orexin neurons recorded from Cx43$^{f/f}$ (n=7 cells, 5 mice) and Cx43 cKO^{GFAP} mice (n=8 cells, 4 mice; Mann-Whitney test, ***p<0.001) recorded in the whole-cell current-clamp mode. (D) Loose patch-clamp recording of spontaneous firing in an orexin neuron from Cx43$^{f/f}$ mouse. (E) Same experiment as in (D) but in an orexin neuron from Cx43 cKO^{GFAP} mouse. (F) Average firing rate of orexin neurons recorded from Cx43$^{f/f}$ (n=7 cells, 4 mice) and Cx43 cKO^{GFAP} mice (n=6 cells, 3 mice; Mann-Whitney test, ***p<0.001) in loose patch-clamp configuration. (G) Whole-cell current-clamp recordings performed in ACSF containing 2.5mM glucose showing the membrane response of an orexin neuron from Cx43$^{f/f}$ (left) and Cx43 cKO^{GFAP} mice (right) to a positive current ramp from 0 to 50pA (5s). (H) Average instantaneous frequency of orexin neurons from Cx43$^{f/f}$ (n=15 cells, 9 mice) and Cx43 cKO^{GFAP} mice (n=11 cells, 7

mice; ANOVA followed by post-hoc test, *p<0.05, **p<0.01, ***p<0.001) in 5pA bins during the incremental current injection. See also Figure S2.

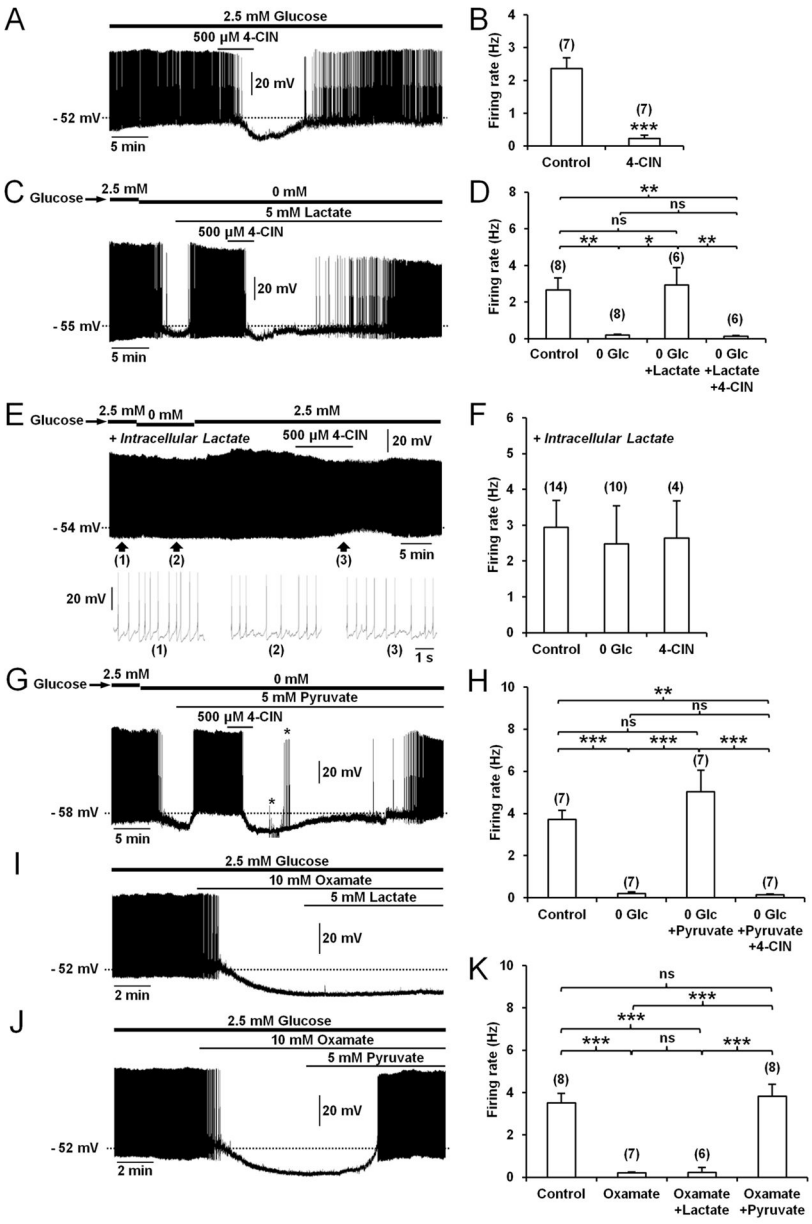

Figure 3. Endogenous production of lactate sustains spontaneous activity of orexin neurons

(A) Whole-cell current-clamp recording performed in ACSF containing 2.5mM glucose showing that bath application of the MCTs inhibitor, 4-CIN, hyperpolarized and decreased the firing rate of an orexin neuron from $Cx43^{f/f}$ mouse. (B) Summary of the 4-CIN effect on the firing rate of orexin neurons from $Cx43^{f/f}$ mice (n=7 cells, 3 mice; paired Student t test, ***p<0.001). (C) Whole-cell current-clamp recording showing that a switch from 2.5 to 0mM glucose hyperpolarized and decreased the firing rate of an orexin neuron from $Cx43^{f/f}$ mouse. On the same neuron, lactate reversed the glucose deprivation effect and this effect was cancelled by 4-CIN. (D) Average firing rate of orexin neurons from $Cx43^{f/f}$ mice in different conditions (in 2.5mM glucose (Control), n=8 cells, 6 mice; in 0mM glucose (0 Glc), n=8 cells, 6 mice; in 0mM glucose with lactate, n=6 cells, 3 mice; in 0mM glucose

with lactate and 4-CIN, n=6 cells, 3 mice; ANOVA followed by post-hoc test, *p<0.05 and **p<0.01; ns, nonsignificant). (E) Intracellular dialysis of 2.5mM lactate (>20min) in an orexin neuron from $Cx43^{f/f}$ mouse through the patch pipette prevented the inhibitory effects of glucose deprivation and 4-CIN. Bottom traces show expanded time scales of the recording at the indicated time points (1), (2) and (3). (F) Average firing rate of orexin neurons from $Cx43^{f/f}$ mice during intracellular dialysis of 2.5mM lactate in 2.5mM glucose (Control, n=14 cells, 8 mice), 0mM glucose (0 Glc, n=10 cells, 6 mice) and 2.5mM glucose with 4-CIN (4-CIN, n=4 cells, 3 mice; ANOVA, p>0.05). (G) Whole-cell current-clamp recording of an orexin neuron from $Cx43^{f/f}$ mouse showing that bath application of the downstream metabolite of LDH, pyruvate, reversed the inhibitory effect of glucose deprivation. Pyruvate effect was suppressed by 4-CIN. Asterisks indicate the time of application of hyperpolarizing and depolarizing current pulses to trace current–voltage relationships. (H) Average firing rate of orexin neurons from $Cx43^{f/f}$ mice in different conditions (in 2.5mM glucose (Control); in 0mM glucose (0 Glc); in 0mM glucose with pyruvate; in 0mM glucose with pyruvate and 4-CIN; n=7 cells, 3 mice for each condition, ANOVA followed by post-hoc test, **p<0.01 and ***p<0.001; ns, nonsignificant). (I) Whole-cell current-clamp recording showing that the LDH inhibitor, oxamate, hyperpolarized and decreased the firing rate of an orexin neuron from $Cx43^{f/f}$ mouse in ACSF with 2.5mM glucose. On the same neuron, lactate, the upstream substrate of LDH, did not reverse the inhibitory effect of oxamate. (J) Whole-cell current-clamp recording of an orexin neuron from $Cx43^{f/f}$ mouse showing that pyruvate reversed the inhibitory effect of oxamate. (K) Average firing rate of orexin neurons from $Cx43^{f/f}$ mice in different conditions (in 2.5mM glucose (Control), n=8 cells, 3 mice; in 2.5mM glucose with oxamate (Oxamate), n=7 cells, 3 mice; in 2.5mM glucose with oxamate and lactate (Oxamate+Lactate), n=6 cells, 3 mice; in 2.5mM glucose with oxamate and pyruvate (Oxamate+Pyruvate), n=8 cells, 3 mice; ANOVA followed by post-hoc test, ***p<0.001; ns, nonsignificant). See also Figure S3.

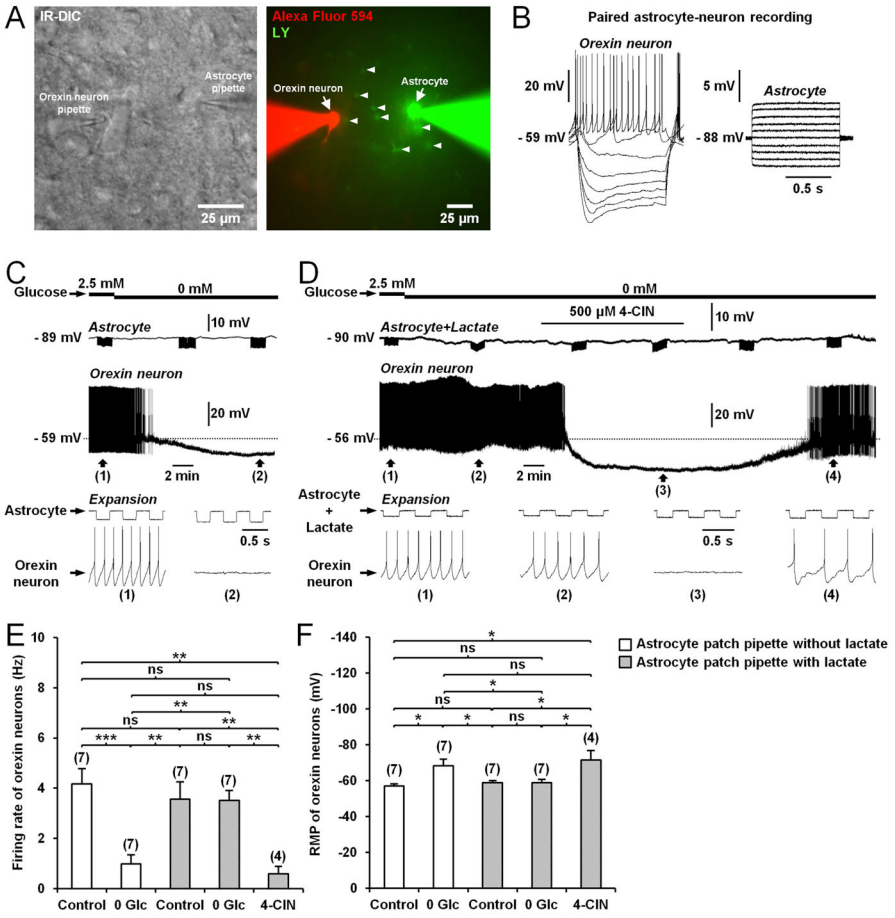

Figure 4. Lactate supply through the astrocytic network sustains the activity of orexin neurons during glucose deprivation

(A) Left: Infrared differential interference contrast (IR-DIC) image of a paired astrocyte-orexin neuron whole-cell recording in the LHA from Cx43$^{f/f}$ mouse. Right: Fluorescence image of the orexin neuron-astrocyte pair shown in the left picture, filled through the pipette with Alexa Fluor 594 (red) and Lucifer yellow (LY, green), respectively. Note the diffusion of LY to neighboring astrocytes (arrowheads). (B) Responses of the cells recorded in (A) to current pulses from −60 to 10pA (1s, 10pA steps) for the orexin neuron and from −200 to 250pA (1s, 50pA steps) for the astrocyte. (C) Representative paired astrocyte-neuron recording from Cx43$^{f/f}$ mouse showing that glucose deprivation inhibits the orexin neuron firing rate. Downward deflections in the astrocyte trace are membrane potential responses to current pulses (−100pA at 2Hz for 80s) to monitor input resistance. (D) Intracellular delivery of lactate (5mM) to astrocyte (Astrocyte+Lactate) through the patch pipette for at least 20min prevents the inhibitory effect of glucose deprivation on the orexin neuron firing rate. This preventive effect was abolished by bath application of 4-CIN. (E and F) Average firing frequency (E) and resting membrane potential (RMP; F) of orexin neurons from Cx43$^{f/f}$ mice exposed to different conditions (during patch-clamp recording of astrocyte not filled with lactate: in 2.5mM glucose (Control), n=7 cells, 5 mice; in 0mM glucose (0 Glc), n=7 cells, 5 mice; during patch-clamp recording of astrocyte filled with 5mM lactate: in 2.5mM glucose (Control), n=7 cells, 4 mice; in 0mM glucose (0 Glc), n=7 cells, 4 mice; in 500µM

4-CIN, n=4 cells, 4 mice; ANOVA followed by post-hoc test, *p<0.05, **p<0.01 and ***p<0.001; ns, nonsignificant).

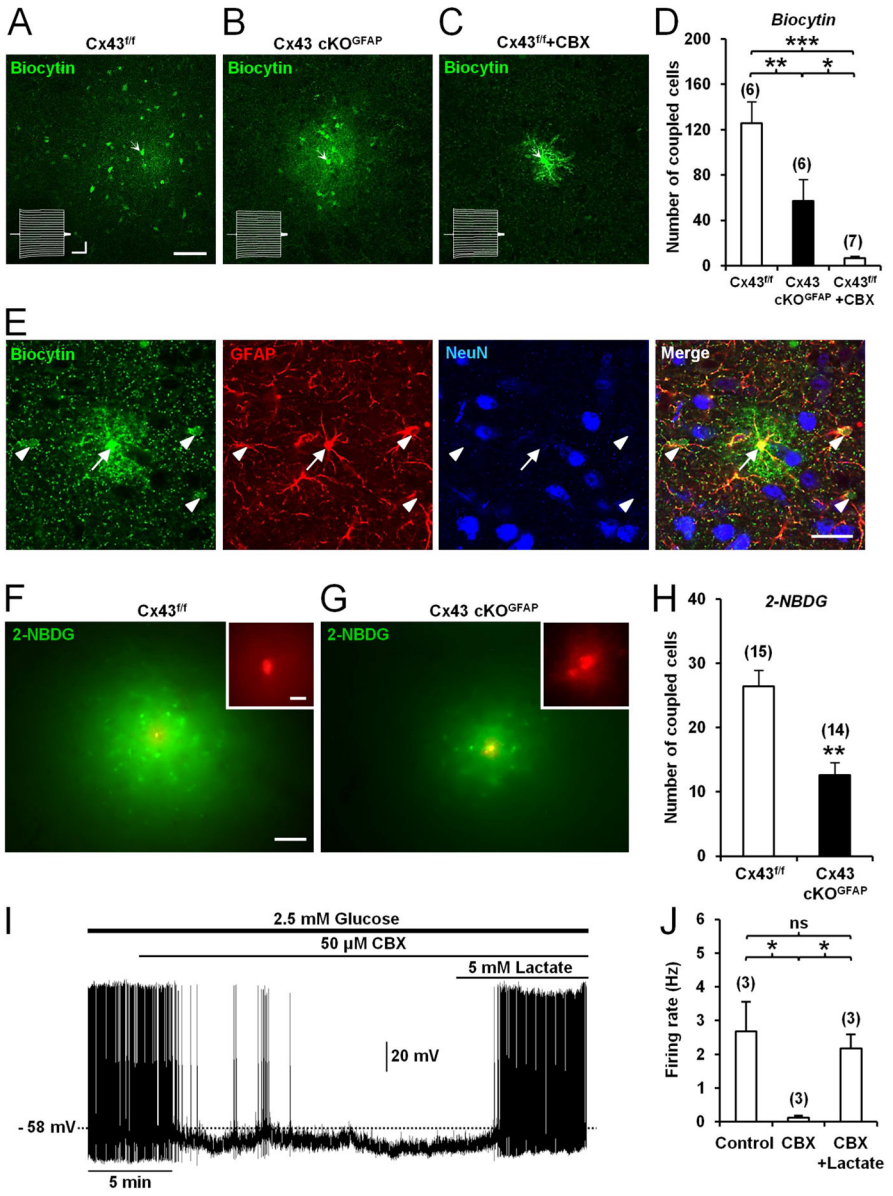

Figure 5. Deletion of Cx43 in astrocytes alters metabolic networks of interconnected astrocytes in the LHA

(A) Functional coupling of astrocytes in the LHA from a Cx43$^{f/f}$ mouse observed by injection of biocytin (20min, green) in a single astrocyte (arrow) through the patch pipette. Biocytin diffusion was revealed with streptavidin after slice fixation. Scale bar: 50µm. Inset shows current traces in the patched astrocyte (arrow) while holding membrane potential at −80mV in response to a series of voltage pulses from −100 to +100mV (300ms, 10mV steps). Calibration bars: 4nA, 100ms. (B) Same experiment as in (A) but in an orexin neuron from Cx43 cKO^{GFAP} mouse. (C) Treatment of slices from Cx43$^{f/f}$ mice with the gap junction channel blocker, carbenoxolone (CBX, 50µM, >15min), abolished intercellular diffusion of biocytin (green) between LHA astrocytes, revealing fine astrocytic processes. (D) Summary of the number of coupled cells recorded in Cx43$^{f/f}$ (n=6, 2 mice), Cx43

cKO^{GFAP} (n=6, 3 mice) and Cx43$^{f/f}$ slices treated with CBX (Cx43$^{f/f}$ + CBX, n=7, 2 mice; ANOVA followed by post-hoc test, *p<0.05, **p<0.01 and ***p<0.001). (E) Dye coupling of LHA astrocytes from Cx43$^{f/f}$ mouse performed with biocytin (green) injected in a single astrocyte (arrow) through the patch pipette and combined with a double immunofluorescence staining for GFAP (red) and NeuN (blue). Scale bar: 50μm. (F) Spread through astrocytic network of the fluorescent glucose analog, 2-NBDG (green), injected in a single LHA astrocyte from Cx43$^{f/f}$ mouse through the patch pipette (20min). Scale bar: 100μm. The injected astrocyte was localized by simultaneously injecting the gap junction-impermeable dye, dextran tetramethylrhodamine (red, inset). Scale bar: 10μm. (G) Same experiment as in (F) but in Cx43 cKO^{GFAP} mouse. (F). Summary of the extent of astrocytic coupling in the LHA for the 2-NBDG in Cx43$^{f/f}$ (n=15 slices, 5 mice) and Cx43 cKO^{GFAP} mice (n=14 slices, 4 mice; Mann-Whitney test, **p<0.01). (I) Whole-cell current-clamp recording showing that CBX hyperpolarized and decreased the firing rate of an orexin neuron from Cx43$^{f/f}$ mouse bathed in ACSF with 2.5mM glucose. On the same neuron, addition of lactate reversed the inhibitory effect of CBX. (J) Average firing rate of orexin neurons from Cx43$^{f/f}$ mice in different conditions (in 2.5mM glucose (Control); in 2.5mM glucose with CBX (CBX); in 2.5mM glucose with CBX and lactate (CBX + Lactate), n=3 cells, 3 mice for each condition; ANOVA, *p<0.05; ns, nonsignificant). See also Figure S4.

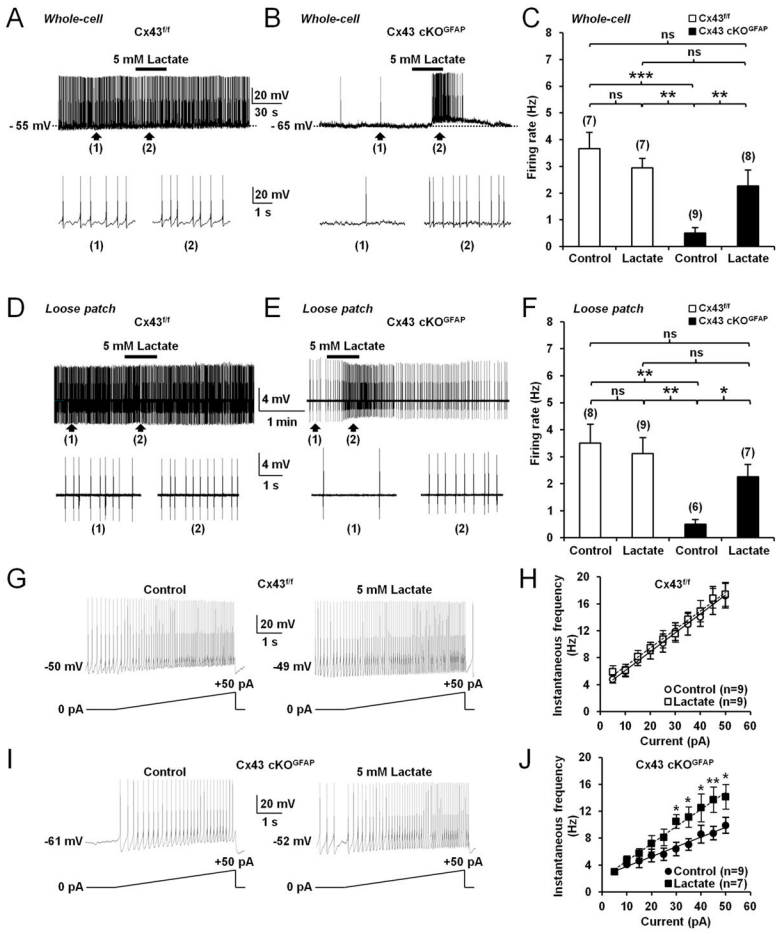

Figure 6. Lactate restores spontaneous firing frequency and excitability of orexin neurons from Cx43 cKO^{GFAP} mice

(A) Whole-cell current-clamp recording showing that bath application of 5mM lactate (equicaloric to 2.5mM glucose) had no effect on the membrane potential and firing rate of an orexin neuron from Cx43$^{f/f}$ mouse bathed in ACSF with 2.5mM glucose. (B) Same experiment as in (A) showing that lactate depolarized and accelerated the firing rate of an orexin neuron from Cx43 cKO^{GFAP} mouse. (C) Average firing rate of orexin neurons recorded in whole-cell current-clamp mode while bathed in ACSF with 2.5mM glucose in the presence and absence of lactate among genotypes (Cx43$^{f/f}$ without lactate (Control), n=7 cells, 4 mice; Cx43$^{f/f}$ with lactate, n=7 cells, 3 mice; Cx43 cKO^{GFAP} without lactate (Control), n=9 cells, 4 mice; Cx43 cKO^{GFAP} with lactate, n=8 cells, 4 mice; ANOVA followed by post-hoc test, **p<0.01 and ***p<0.001; ns, nonsignificant). (D) Loose patch-clamp recording showing that lactate did not have any effect on the firing of an orexin neuron from Cx43$^{f/f}$ mouse in ACSF with 2.5mM glucose. (E) Same experiment as in (D) showing that lactate increased firing frequency of an orexin neuron from Cx43 cKO^{GFAP} mouse. (F) Average firing rate of orexin neurons recorded in loose patch configuration in different genotypes and conditions (Cx43$^{f/f}$ without lactate (Control), n=8 cells, 4 mice; Cx43$^{f/f}$ with lactate, n=9 cells, 4 mice; Cx43 cKO^{GFAP} without lactate (Control), n=6 cells, 3 mice; Cx43 cKO^{GFAP} with lactate, n=7 cells, 3 mice; ANOVA followed by post-hoc test,

*p<0.05 and **p<0.01; ns, nonsignificant). (G) Whole-cell current-clamp recording in ACSF with 2.5mM glucose showing the membrane response of an orexin neuron from $Cx43^{f/f}$ mouse to a positive current ramp from 0pA to 50pA (5s) in the absence (Control, left) or presence of lactate (right). (H) Average instantaneous frequency of orexin neurons from $Cx43^{f/f}$ mice in 5pA bins during the incremental current injection in the absence (Control, n=9 cells, 4 mice) or presence of lactate (n=9 cells, 5 mice; ANOVA, p>0.05). (I) Same experiments as in (G) showing that lactate increased excitability of an orexin neuron from Cx43 cKO^{GFAP} mouse. (J) Average instantaneous frequency of orexin neurons from Cx43 cKO^{GFAP} mice in 5pA bins during the incremental current injection in the absence (Control, n=9 cells, 4 mice) or presence of lactate (n=7 cells, 3 mice; ANOVA followed by post-hoc test, *p<0.05 and **p<0.01).

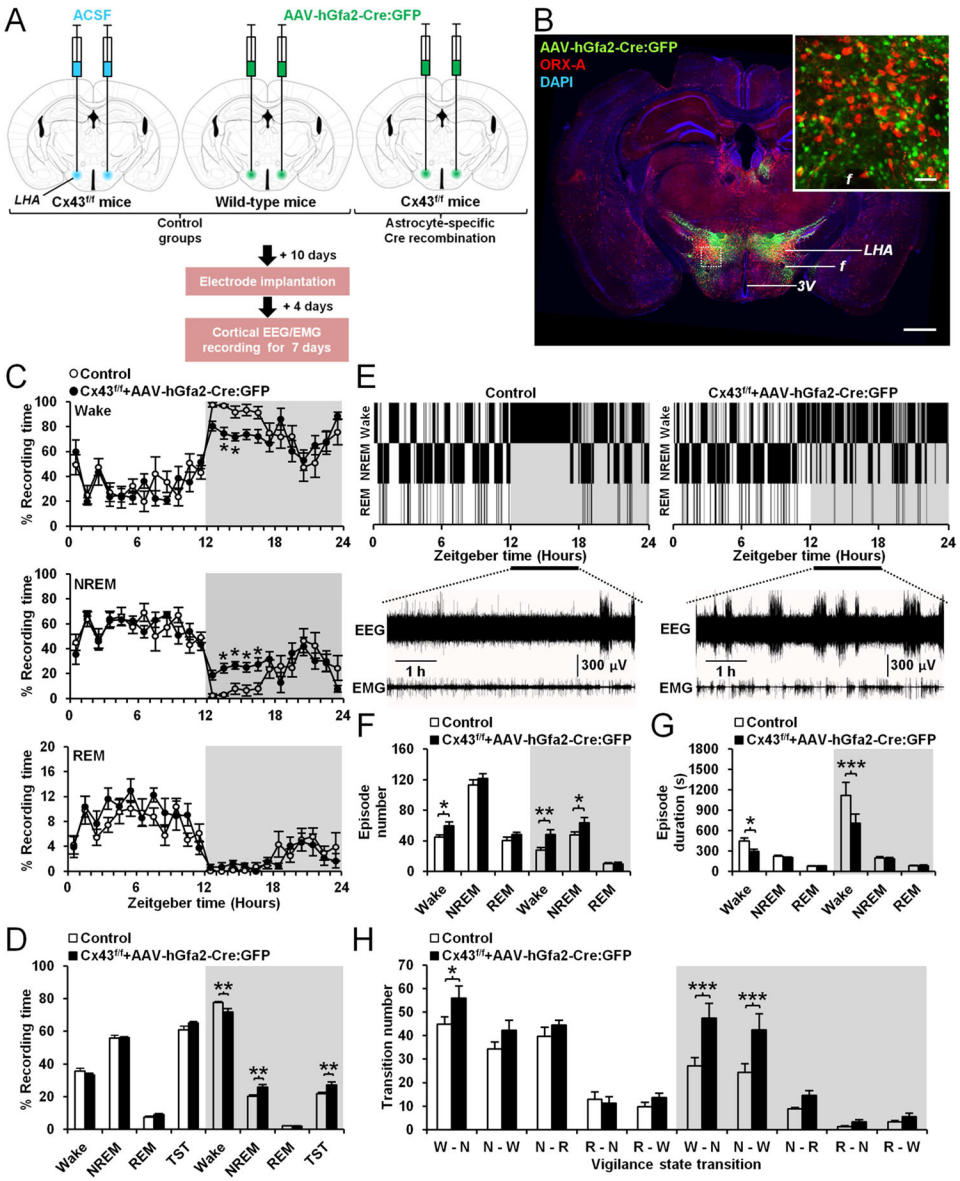

Figure 7. Deletion of Cx43 in astrocytes from the LHA causes sleepiness and instability of wakefulness during the nocturnal active phase

(A) Experimental design and time line. (B) Brain section from a $Cx43^{f/f}$ mouse 21 days after bilateral injection of AAV-hGfa2-Cre:GFP into the LHA showing Cre:GFP expression (green), orexin (ORX)-A immunopositive cells (red) and DAPI nuclear staining (blue). f: fornix, LHA: lateral hypothalamic area, 3V: third ventricle. Scale bar: 500µm. The inset represents a magnification of the area delimited by the dash rectangle. Scale bar: 50µm. (C) Percentage average of the time spent in wake (top), NREM sleep (middle) and REM sleep (bottom) per h in control (n=8) and $Cx43^{f/f}$ mice transduced with AAV 21 days after injections ($Cx43^{f/f}$ + AAV-hGfa2-Cre:GFP, n=8; Wake and NREM sleep: ANOVA followed by post-hoc test, *p<0.05; REM sleep: ANOVA, p>0.05). (D) Averaged percentage of time spent in wake, NREM and REM sleep during the 12h light and dark phases in control (n=8) and $Cx43^{f/f}$ mice transduced with AAV (n=8; ANOVA followed by post-hoc test, **p<0.01).

TST: total sleep time including REM and NREM sleep. (E) Representative hypnograms of a control (left) and $Cx43^{f/f}$ mouse transduced with AAV (right). Bottom traces represent EEG/EMG recordings from ZT12 to ZT18. (F and G) Average of the number (F) and duration (G) of wake, NREM and REM sleep episodes during the 12h light and dark phases in control (n=8) and $Cx43^{f/f}$ mice transduced with the AAV (n=8; ANOVA followed by post-hoc test, *p<0.05, **p<0.01 and ***p<0.001). (H) Average number of transitions between vigilance states (W: Wake, N: NREM, R: REM) in control (n=8) and $Cx43^{f/f}$ mice transduced with AAV (n=8; ANOVA followed by post-hoc test, *p<0.05 and ***p<0.01). See also Figure S5.

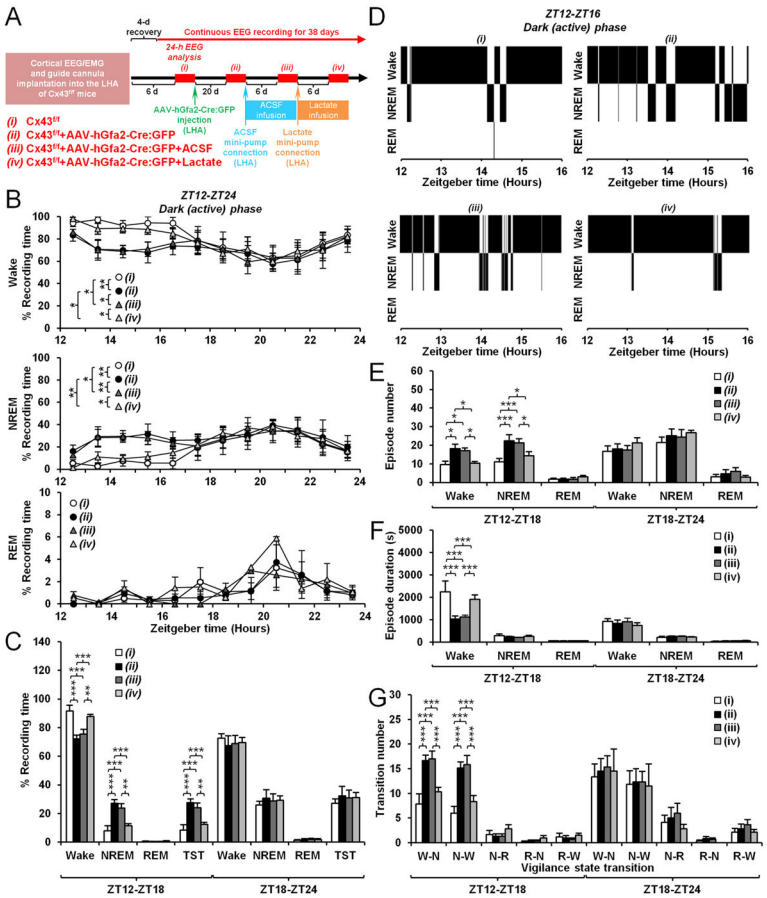

Figure 8. Lactate abrogates nocturnal sleepiness and instability of wakefulness induced by the deletion of Cx43 in astrocytes from the LHA

(A) Experimental design and time line. Twenty-four-h EEG recordings (ZT0-ZT24) were analyzed over time in the same Cx43$^{f/f}$ mouse (n=6) at the 4 experimental time points (i, ii, iii, iv; red bars). (B) Percentage average of the time spent in wake (top), NREM (middle) and REM sleep (bottom) per h during the 12h dark phase at the 4 time points (ANOVA followed by post-hoc test, *p<0.05, **p<0.01 and ***p<0.001). (C) Averaged percentage of time spent in wake, NREM and REM sleep during the first (ZT12-ZT18) and last (ZT18-ZT24) 6h of the dark phase at the 4 time points (ANOVA followed by post-hoc test, **p<0.01 and ***p<0.001). TST: total sleep time including REM and NREM sleep. (D) Representative hypnograms of the same Cx43$^{f/f}$ mouse during the first 4h of the dark phase (ZT12-ZT16) at the 4 time points. (E and F) Average of the number (E) and duration (F) of wake, NREM and REM sleep episodes during the first (ZT12-ZT18) and last (ZT18-ZT24) 6h of the dark phase at the 4 time points (ANOVA followed by post-hoc test, *p<0.05 and ***p<0.001). (G) Average number of transitions between vigilance states (W: Wake, N: NREM, R: REM) during the first (ZT12-ZT18) and last (ZT18-ZT24) 6h of the dark phase at the 4 time points (ANOVA followed by post-hoc test, ***p<0.001).